

AUGUST 2007

Climatology of UV-A, UV-B, and Erythemal Radiation at the Earth's Surface, 1979-2000

J. Lee-Taylor
S. Madronich

ATMOSPHERIC CHEMISTRY DIVISION

NATIONAL CENTER FOR ATMOSPHERIC RESEARCH
BOULDER, COLORADO

NCAR TECHNICAL NOTES

The Technical Note series provides an outlet for a variety of NCAR Manuscripts that contribute in specialized ways to the body of scientific knowledge but that are not suitable for journal, monograph, or book publication. Reports in this series are issued by the NCAR scientific divisions. Designation symbols for the series include:

EDD – Engineering, Design or Development Reports

Equipment descriptions, test results, instrumentation, and operating and maintenance manuals.

IA – Instruction Aids

Instruction manuals, bibliographies, film supplements, and other research, or instructional aids.

PPR – Program Progress Reports

Field program reports, interim and working reports, survey reports, and plans for experiments.

PROC – Proceedings

Documentation or symposia, colloquia, conferences, workshops, and lectures. (Distribution may be limited to attendees.)

STR – Scientific and Technical Reports

Data compilations, theoretical and numerical investigations, and experimental results.

The National Center for Atmospheric Research (NCAR) is operated by the nonprofit University Corporation for Atmospheric Research (UCAR) under the sponsorship of the National Science Foundation. Any opinions, findings, conclusions, or recommendations expressed in this publication are those of the author(s) and do not necessarily reflect the views of the National Science Foundation.

AUGUST 2007

Climatology of UV-A, UV-B, and Erythemal Radiation at the Earth's Surface, 1979-2000

J. Lee-Taylor
S. Madronich

ATMOSPHERIC CHEMISTRY DIVISION

NATIONAL CENTER FOR ATMOSPHERIC RESEARCH
BOULDER, COLORADO

CONTENTS

PREFACE.....	vii
1 INTRODUCTION.....	1
2 METHOD.....	3
3 RESULTS.....	7
3.1 Satellite-derived UV climatologies.....	7
3.2 Comparison with ground-based measurements.....	25
4 CONCLUSIONS.....	27
ACKNOWLEDGEMENTS.....	31
APPENDIX A. ADDITIONAL UV WEIGHTING FUNCTIONS.....	33
APPENDIX B. DATA AVAILABLE FOR DOWNLOAD.....	39
REFERENCES.....	41

LIST OF FIGURES

Figure 1. Climatological daily doses of UV-A at Earth’s surface	8
Figure 2. As Fig. 1, for UV-B.....	9
Figure 3. As Fig. 1, for UV _{ery}	10
Figure 4. Climatological annual mean cloud reduction factors for daily doses of a) UV-A, b) UV-B, and c) UVery	11
Figure 5a. Seasonal variability of daily doses of UV-A, Jan – June	12
Figure 5c. Seasonal variability of daily doses of UV-A, July – Dec	13
Figure 6a. As Fig. 5a, for UV-B.	14
Figure 6b. As Fig. 5b, for UV-B.....	15
Figure 7a. As Fig. 5a, for UV _{ery}	16
Figure 7b. As Fig. 5b, for UV _{ery}	17
Figure 8a. Seasonal variability of UV-A calculated without correcting for the presence of clouds, Jan – Mar	18
Figure 8b. Seasonal variability of UV-A calculated without correcting for the presence of clouds, Apr – Jun	19
Figure 9a. As Fig. 8a, for UV-B.	20
Figure 9b. As Fig. 8b, for UV-B.....	21
Figure 10a. As Fig. 8a, for UV _{ery}	22
Figure 10b. As Fig. 8b, for UV _{ery}	23
Figure 11. Changes in average daily erythemal UV doses between the periods 1979-1989 and 1990-2000.	24
Figure 12. Comparison of yearly-averaged daily erythemal UV doses derived from satellite observations with those derived from ground-based measurements at 21 stations.	26
Figure 13. Differences between ground-based and satellite-derived annual mean daily erythemal UV doses.....	27
Figure A1a. Seasonal variability of daily doses of UV weighted for previtamin D ₃ production in human skin, Jan – Mar.	34
Figure A1b. As Fig. A1a, for April – June.	35
Figure A2a. As Fig. A1a, for UV weighted for non-melanoma carcinogenesis in human skin: Jan – Mar.....	36
Figure A2b. As Fig. A2a, for April – June.	37
Figure B1. Example data file	39

PREFACE

Solar ultraviolet (UV) radiation reaching Earth's surface is of interest because of its role in the induction of various biological and chemical processes, including skin cancer. The purpose of this Technical Note is to make available climatological distributions of monthly mean surface-level UV, calculated using the NCAR radiative transfer model TUV (Tropospheric Ultraviolet-Visible), and using as input the ozone column amounts and cloud reflectivities (at 380 nm) measured by satellite instruments (TOMS, Total Ozone Mapping Spectrometer, aboard Nimbus-7, Meteor-3, and Earth Probe). The climatology is averaged over the years 1979-2000, for UV-A (315-400 nm), UV-B (280-315 nm), and erythemal (skin-reddening) radiation. Coverage is global, excluding the poles. Comparisons with direct ground-based measurements archived at the World Ozone and Ultraviolet Data Center show agreement at the 10-20% level, except at high latitudes where the large surface albedo of snow and ice invalidates the use of satellite-observed reflectivity in estimating cloud cover. The data may be helpful in assessing the role of long-term environmental exposure to ultraviolet radiation, e.g., in epidemiological studies of skin cancer.

Climatologies are presented in Appendix A of two additional response functions for the interaction of UV radiation with human skin: synthesis of previtamin D3, and non-melanoma carcinogenesis. The data and detailed figures of the climatologies presented here are available online via the Community Data Portal at the National Center for Atmospheric Research. Access instructions are supplied in Appendix B.

This Technical Note is revised from the previous version (dated July 2007). The climatologies for Previtamin D3 Production and Non-melanoma Carcinogenesis given in that version were calculated with an inadvertently high ground albedo. The calculations presented here all use a global albedo of 0.05, resulting in significant corrections to the climatologies of Previtamin D3 Production and Non-melanoma Carcinogenesis. All climatologies have now been updated to TOMS Version 8 data, and some minor bugs have been corrected. The Version 8 UV-A, UV-B, and Erythemal UV climatologies are generally similar to Version 7, although the inter-decadal differences between the climatologies have increased by a couple of percentage points. An error in the equations on page 3 has been corrected.

1 INTRODUCTION

Solar ultraviolet (UV) radiation transmitted through the atmosphere to Earth's surface is known to induce various biological and chemical processes, many of which are harmful to living tissues and some materials (see *UNEP*, [2003] for a review). The geographical distribution of surface UV radiation is of considerable interest towards understanding these effects. However, environmental UV levels are highly variable due to cyclic changes in solar elevation and Earth-Sun distance, and to variations in atmospheric transmission (mainly from ozone, clouds, and aerosols) and surface reflections. UV radiation measurements by ground-based instruments are too few, and their record relatively short, to construct a unified picture of its average global distribution.

An alternate method of estimating surface UV levels with long-term global coverage relies on satellite-based observations of the Earth's atmosphere and surface, combined with a computer model of the propagation of UV radiation through the atmosphere. This methodology has already been applied to interesting aspects of the problem, such as estimation of zonal mean irradiances at different UV wavelengths, of trends due to ozone changes, of cloud effects, and of geographical distributions based on monthly averaged ozone and clouds [e.g., *Frederick and Lubin*, 1988; *Madronich*, 1992; *Eck et al.*, 1995; *Frederick and Erlick*, 1995; *Herman et al.*, 1996, 1999; *Lubin et al.*, 1998; *Sabziparvar et al.*, 1999; *Herman et al.*, 2000; *McKenzie et al.*, 2001]. Here, satellite-based observations of atmospheric ozone and clouds are used to derive a climatology of erythemal UV radiation with nearly global coverage (excluding the polar regions), averaged over the years 1979-2000. A fast method has been developed for the explicit calculation of UV daily doses for each day of the whole time period. Averaging daily UV doses, rather than calculating monthly doses on the bases of monthly-averaged cloudiness and ozone, reduces possible uncertainties connected with the non-linear relationship between atmospheric parameters (e.g., total ozone and clouds) and surface UV radiation. Comparisons with long-term measurements at 22 UV monitoring stations allow some assessment of the reliability of this technique.

2 METHOD

The UV broadband irradiances (W m^{-2}) were computed using the TUV (Tropospheric Ultraviolet – Visible) model [Madronich and Flocke, 1997], as integrals over wavelength λ (nm) of spectral irradiances $E(\lambda)$ ($\text{W m}^{-2}\text{nm}^{-1}$) weighted by appropriate spectral functions $S(\lambda)$ (unit-less):

$$\text{Irradiance} = \int S(\lambda) E(\lambda) d\lambda$$

$E(\lambda)$ is a function of solar zenith angle and surface elevation, as well of as optical depth profiles of atmospheric absorbers and scatterers (e.g., ozone and clouds). For UV-A and UV-B, the values of $S(\lambda)$ are unity in the respective wavelength ranges 315-400 nm and 280-315 nm, and zero outside these ranges. For erythemal radiation, $S(\lambda)$ is the CIE (Commission Internationale de l'Eclairage) erythemal sensitivity function (action spectrum) given by McKinlay and Diffey [1987], and is represented by:

$$\begin{aligned} \log_{10} S_{\text{ery}}(\lambda) &= 0.0 && (250-298 \text{ nm}) \\ &= 0.094(298 - \lambda) && (298-328 \text{ nm}) \\ &= 0.015(139 - \lambda) && (328-400 \text{ nm}). \end{aligned}$$

The use of this action spectrum has been accepted for the calculation of the instantaneous UV index (defined as the UVery irradiance multiplied by 40 [see ICNRP, 1995; WMO, 1997]), and the time-integrated standard erythemal dose ($\text{SED} = 100 \text{ J m}^{-2}$ [see CIE, 1998]). In practice, use of this CIE spectrum emphasizes the ozone-sensitive region 295-320 nm, peaking near 305 nm, with minor contributions from longer wavelengths, as shown by Madronich *et al.* [1998] (see their Fig. 1).

The compilation of a global UV climatology is computationally intensive, requiring the calculation of $E(\lambda)$ at all relevant wavelengths, at each geographical location, over diurnal cycles for each day of each year. To reduce computational time, we pre-tabulated values of the UV-A, UV-B, and erythemal irradiances as a function of solar zenith angle (0° to 110° in 1° steps), ozone column (43 to 643 DU in steps of 10 DU), and surface elevation (0, 3, and 8 km above sea level), for cloud-free and aerosol-free conditions. $E(\lambda)$ at the Earth's surface was computed at 1 nm steps from 280 to 400 nm. The spectral irradiance incident at the top of the atmosphere was taken from the Atlas3/SUSIM measurements [D. Prinz, priv. comm., 1998]. Vertical profiles, appropriate for mid-latitude annual average conditions, for air density, temperature, and ozone were taken from the US Standard Atmosphere [USSA, 1976]. The ozone profile was re-scaled to the actual ozone column, see below. The propagation of solar radiation through the atmosphere was computed with a 4-stream discrete ordinates method [Stamnes *et al.*, 1988], with pseudo-spherical correction for improved accuracy at low Sun conditions [Petropavlovskikh, 1995]. A Lambertian surface albedo of 5% was assumed at all wavelengths.

The atmospheric ozone column and cloud reflectivity at 380 nm (R) were taken from the Total Ozone Mapping Spectrometer (TOMS) from three satellites: Nimbus-7, Level 3/Version 8 [McPeters *et al.*, 1996], 1 Nov. 1978 to 31 Dec. 1992; Meteor-3, Level 3/Version 8 [Herman *et al.*, 1996], 22 Aug. 1991 to 11 Dec. 1994; and Earth Probe, Level 3/Version 8 [McPeters *et al.*, 1998], 7 Jul. 1996 to 30 Jun. 2000. The geographical resolution of the measurements was 1.25° longitude by 1.00° latitude. For each grid point, only one satellite overpass per day occurred (*ca.* local noon). We therefore assumed constant ozone and reflectivity values for the entire day. Local values of the

ozone column, solar zenith angle and surface elevation were used to compute the clear-sky irradiances at 30 minute intervals over half days by interpolation of the pre-tabulated values. Assuming symmetry about noon, these data were integrated over 24 hours to obtain the daily UV-A, UV-B, and erythemal doses. A correction for variations in the Earth-Sun distance was applied as a function of date. A reduction factor F for cloud cover, identical to that used by *Eck et al.* [1995], was then applied:

$$\begin{aligned} 1 / F &= [1 - (R - 0.05)/0.9] && (R \leq 50\%) \\ &= (1 - R) && (R > 50\%). \end{aligned}$$

For cloud-free and aerosol-free conditions, total reflectivity at 380 nm is dominated by Rayleigh scattering and surface reflections, the latter being rather small at UV wavelengths unless snow or ice is present. The TOMS algorithm attributes excess reflectivity to clouds or scattering aerosols, without distinguishing between the two. When high surface albedo is encountered (e.g., snow or ice), this method erroneously interprets the high surface reflectivity as cloud cover, thus artificially reducing surface UV irradiance. Polar regions are therefore excluded from our analysis. For all other locations, monthly averaged erythemal doses were computed but were invalidated if missing data as described below.

The calculation of UV doses should in principle be carried out for each location and each day over the satellite record (ca. 1979-2000). However, gaps in the satellite record exist, so that for some days and/or locations, no doses could be computed. These missing days require some consideration to avoid biases in any long term averages and trends. For each location, monthly average doses were calculated for each of the 247 months in the combined dataset, but were considered valid only if at least half of the days in that month had data. No attempt was made to discriminate between months on which data gaps occurred mostly in the early part of the month, and those with gaps mostly during the later part of the month. In some cases, measurements for the same location and days were available from two different satellites: in this case, monthly means for each satellite were computed, then averaged together to obtain a single mean for that month.

Climatological monthly values were computed for each location by averaging all valid values for that month over multiple years (e.g. climatological January is the mean of all valid January values over 1979-2000, etc.). For most of this report, we consider averages over the full 22 years (1979-2000), but for some of the discussion below we also considered separately the time periods 1979-1989 and 1990-2000. Climatological annual values were computed as the mean of all valid climatological monthly values, specifically (mean of all Jans. + mean of all Febs. + ... + mean of all Decs.) / 12.

The second period (1990-2000) is missing some data (all of 1995, 1996 Jan-Jun, 2000 Jul-Dec). We tested the effects of these missing data on the calculated changes by temporarily removing the analogous months from the 1979-1989 climatology and comparing the resulting climatology to that of the complete 1979-1989 period. Differences of $<\pm 0.2\%$ were obtained. This is on the order of $\sim 1/10$ of the clear sky changes between the two periods 79-89 and 90-00, and on the order of $< 1/10$ of the changes in the "all sky" values between the two periods.

For comparison with the satellite-derived estimates, measurements of UV irradiances by ground-based spectroradiometers were used, from the World Ozone and UV Data Center archive [*WOUDC*; data downloaded June 2002]. Measured UV_{ery} doses are reported as daily integrals of spectral observations integrated over wavelength with the *McKinlay and Diffey* [1987] erythemal

action spectrum weighting. The archives include 22 non-polar stations: ten in Canada (Meteorological Service of Canada, MSC), four in Japan (Japan Meteorological Agency, JMA), two in Taiwan (Central Weather Bureau of Taiwan, TWB), and one each at Obninsk, Russia (Institute of Experimental Meteorology - Scientific Production Association, IEM-SPA), Poprad-Ganovce, Slovakia (Slovak HydroMeteorological Institute, SHMI), Mauna Loa, HI (MSC), San Diego, CA, Ushuaia, Argentina, and Palmer Station, Antarctica (all US National Science Foundation, NSF). The NSF sites operated double monochromators (Biospherical Instruments, Inc), while all other sites operated Brewer single monochromators. Our satellite-based irradiance values for station locations were derived for the exact locations and altitudes of the ground-based stations.

Table 1. Details of ground-based stations.

Station	Agency	Station i.d.	Latitude (°)	Longitude (°)	Altitude (m)
Churchill	MSC	77	58.8	-94.1	35.0
Obninsk	IEM-SPA	307	55.12	36.6	0
Edmonton	MSC	21	53.55	-114.1	766
Saskatoon	MSC	241	52.1	-106.7	550.0
Regina	MSC	338	50.21	-104.71	592
Winnipeg	MSC	320	49.9	-97.2	239.0
Poprad-Ganovce	SHMI	331	49.03	20.32	706
Saturna	MSC	290	48.8	-123.1	178.0
Montreal	MSC	319	45.5	45.5	-73.8
Halifax	MSC	321	44.67	-63.57	31
Toronto	MSC	65	43.78	-79.47	198
Sapporo	JMA	12	43.1	141.3	19.0
Tateno	JMA	14	36.1	140.1	31.0
San Diego	NSF	239	32.8	-117.1	0.0
Kagoshima	JMA	7	31.6	130.6	283.0
Naha	JMA	190	26.2	127.67	29
Taipei	TWB	95	25.0	121.5	30.0
Chenkung	TWB	306	23.1	121.37	10
Mauna Loa	MSC	31	19.53	-155.58	3397
Ushuaia	NSF	339	-54.49	-68.19	7
Palmer	NSF	292	-64.46	-64.03	0

3 RESULTS

3.1 Satellite-derived UV climatologies

Figures 1a – 3a show the geographical distribution of daily doses of UV-A , UV-B, and UV_{ery} radiation averaged over the entire time period (1 Nov. 1978 - 30 Jun. 2000). These values include both the effect of ozone and of clouds, as estimated from TOMS data, and are thus assessed to be nearest to the actual values experienced over this time period. Figures 1b – 3b show climatological distributions estimated for hypothetical cloud-free skies (i.e. estimated from the ozone distributions without correcting for the presence of clouds).

As expected, highest doses are generally seen in the tropics, up to ca. $6 \text{ kJ m}^{-2} \text{ day}^{-1}$ (60 SED day^{-1}) for UV_{ery} in the eastern Pacific and eastern Africa, but with substantial cloud-related reductions over western South America, parts of west Africa, and just north of the Equator in the eastern and central Pacific. Middle latitudes of both hemispheres show a general pole-ward decrease from about 5 to $1 \text{ kJ m}^{-2} \text{ day}^{-1}$, with some local highs associated with higher elevations, smaller ozone columns, and infrequent cloudiness (e.g., the Andes mountains, the Tibetan plateau, central Mexico, and the southwestern US), while lower values for those latitudes are noted for east Asia and the coastal eastern Pacific, associated with more frequent cloud cover. Figure 4 shows the cloud reduction factor, calculated as the ratio of the cloud-corrected climatological daily UV dose (Figs. 1a – 3a) to the climatological daily dose calculated without cloud-correction (Figs. 1b – 3b).

The 22-year climatologies of monthly averaged UV doses are shown in Figures 5 – 7. The latitudinal distributions are generally consistent with the annual variation of the subsolar point in the tropics, giving strong seasonal variations at temperate latitudes (out of phase by 6 months between the two hemispheres). The influences of solar position and ozone distribution can more clearly be seen in Figures 8 – 10, the monthly averaged surface UV doses for hypothetical cloud-free conditions. The zonally homogeneous distribution of cloud-free UVA (Fig. 8) shows almost exclusive dependence on solar position, with only small variations due to surface topography, while ozone column variations induce additional zonal variations in the distributions of cloud-free UVB and UV_{ery} (Figs. 9 and 10). The strongest longitudinal variations in the surface UV dose rate distributions are however caused by climatological cloud distributions (Figures 5 – 7).

Detailed analysis of temporal trends is beyond the scope of this work, but some indications may be obtained by comparing the climatological values averaged over 1990-2000 with those averaged over 1979-1989. Figure 11c shows the changes in erythemal doses between these two 11-year periods. Significant changes are seen to have occurred, with annual mean dose rate increases of 8% or more in some regions, including north-central Europe, the eastern seaboard of the US, Siberia, and the Antarctic Ocean. Other regions experienced annual mean dose rate reductions of up to 6%. The dose rate changes are the sum of the effects of changes in ozone column (Fig. 11a) and changes in cloudiness (Fig. 11b). Figure 11a shows clearly the increase in surface UV resulting from stratospheric ozone reductions, not only in the Antarctic region, but also at mid-latitudes. Figure 14b shows a reduction in cloudiness maximizing over north-central Europe, possibly as a result of the introduction of cleaner fuel-burning technologies in the west, combined with a contraction of heavy industry in the east. Increases in cloudiness are seen over the Bay of Bengal, and over the Humboldt Current off the west coast of South America, possibly owing to the

enhanced El Niño conditions prevalent during the 1990s. The apparent reductions in cloudiness around the coasts of southern Alaska and Hudson Bay are likely artifacts related to decadal-scale changes in snow and ice cover.

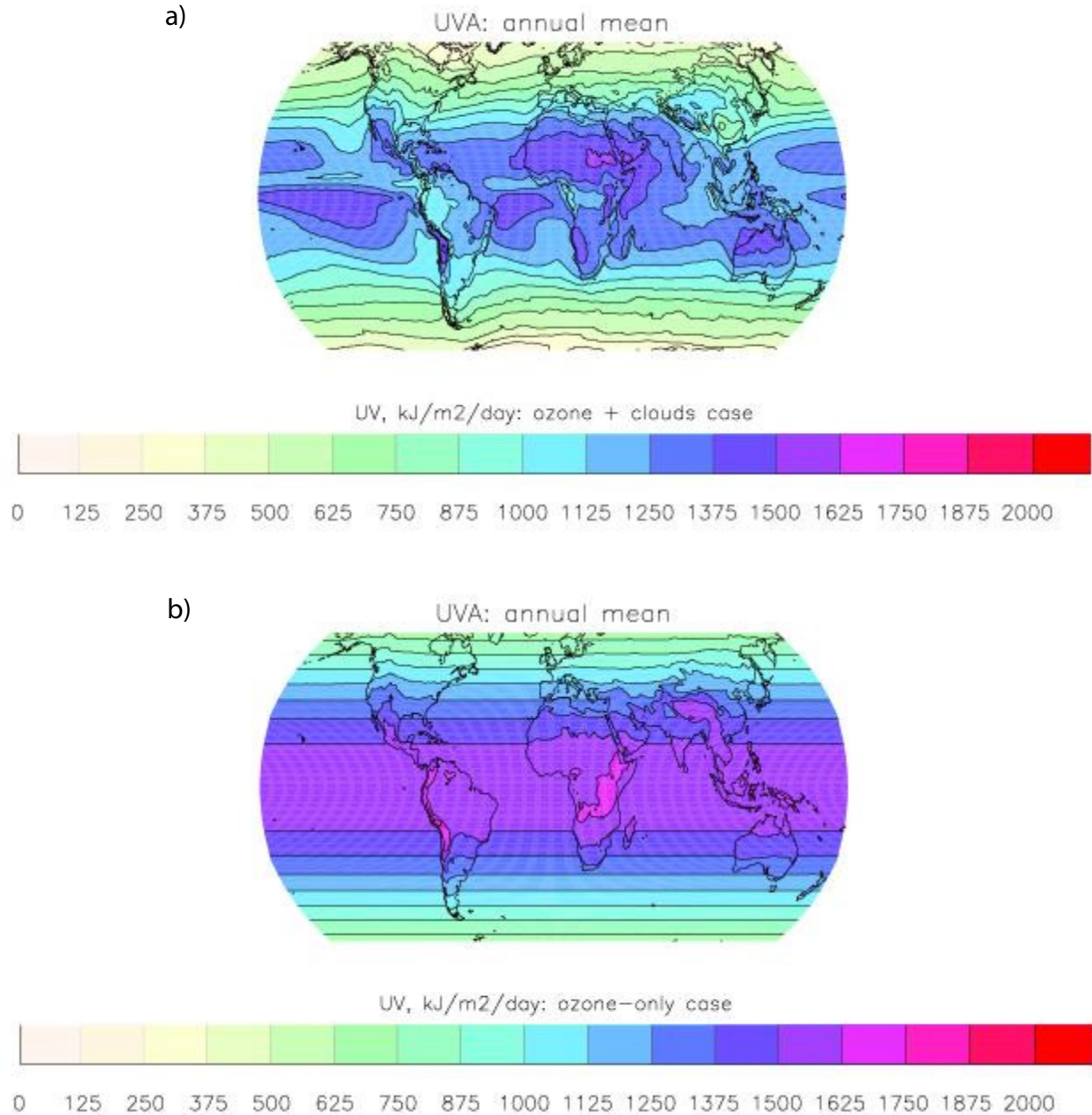


Figure 1. Climatological daily doses of UV-A at Earth's surface, derived from satellite (TOMS) observations of the atmospheric ozone column and cloud reflectivity at 380 nm and averaged annually over Nov 1, 1978 – Jun 30, 2000, a) with and b) without correcting for the presence of clouds.

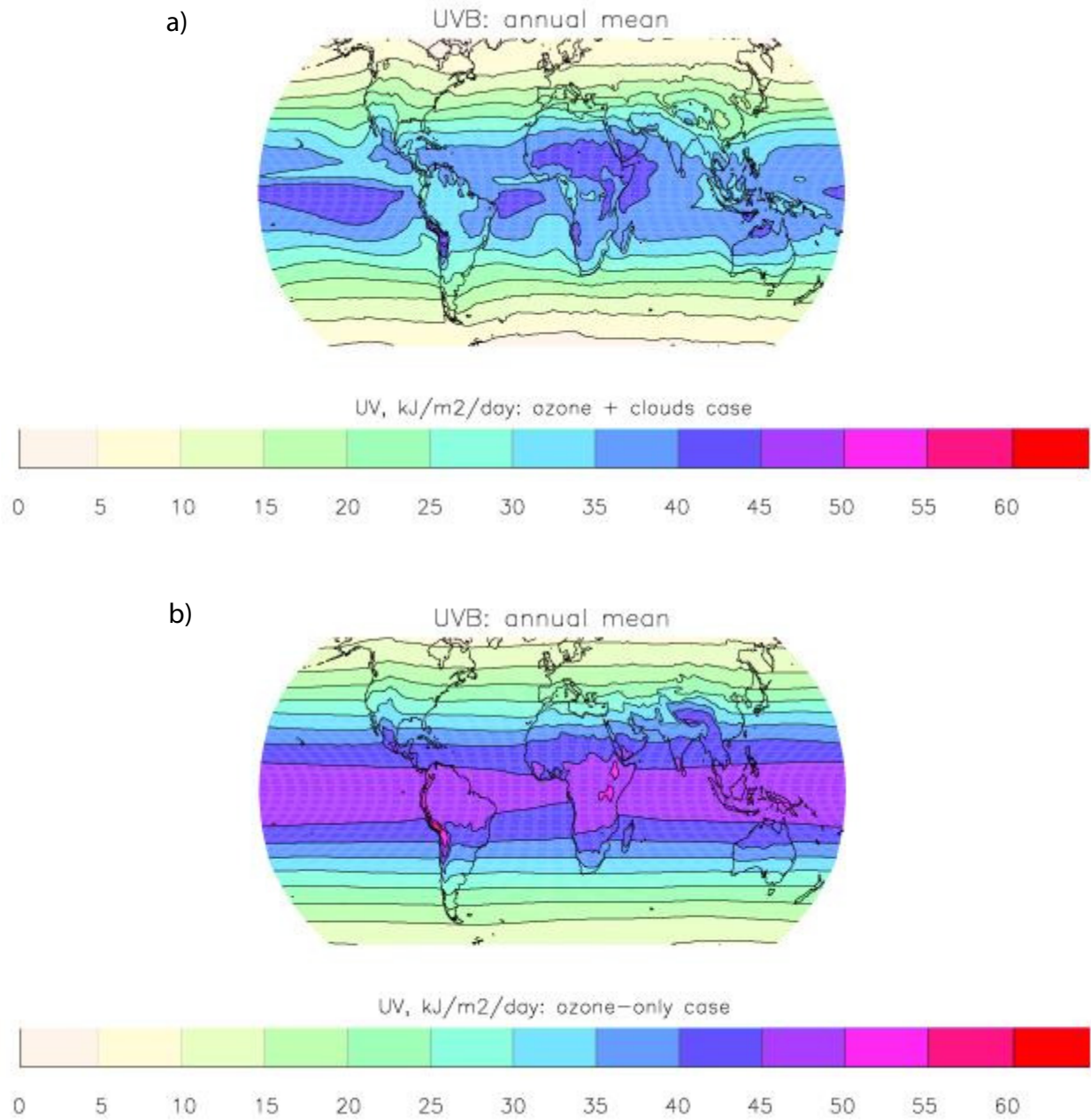


Figure 2. As Fig. 1, for UV-B.

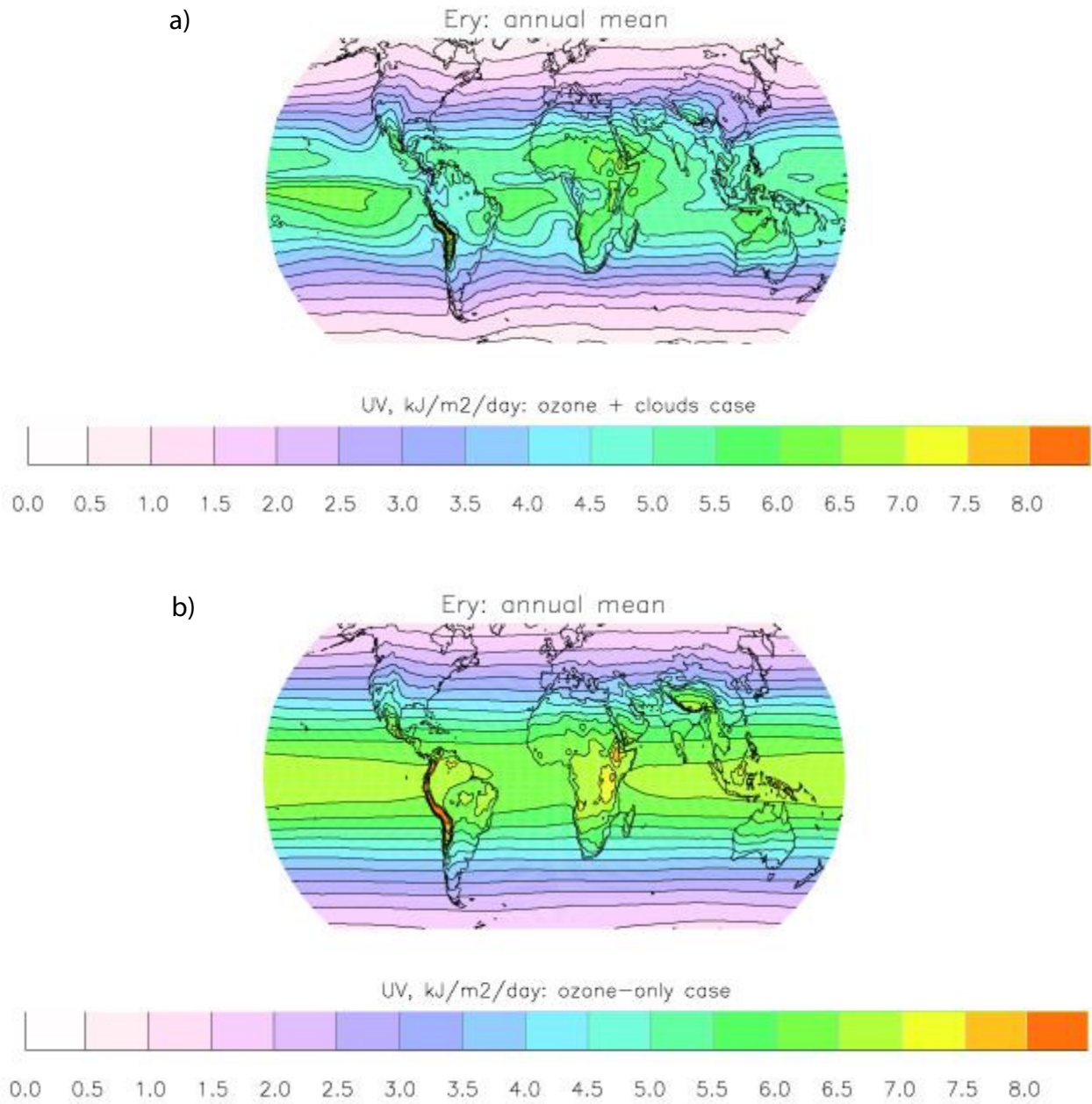


Figure 3. As Fig. 1, for UV_{ery} .

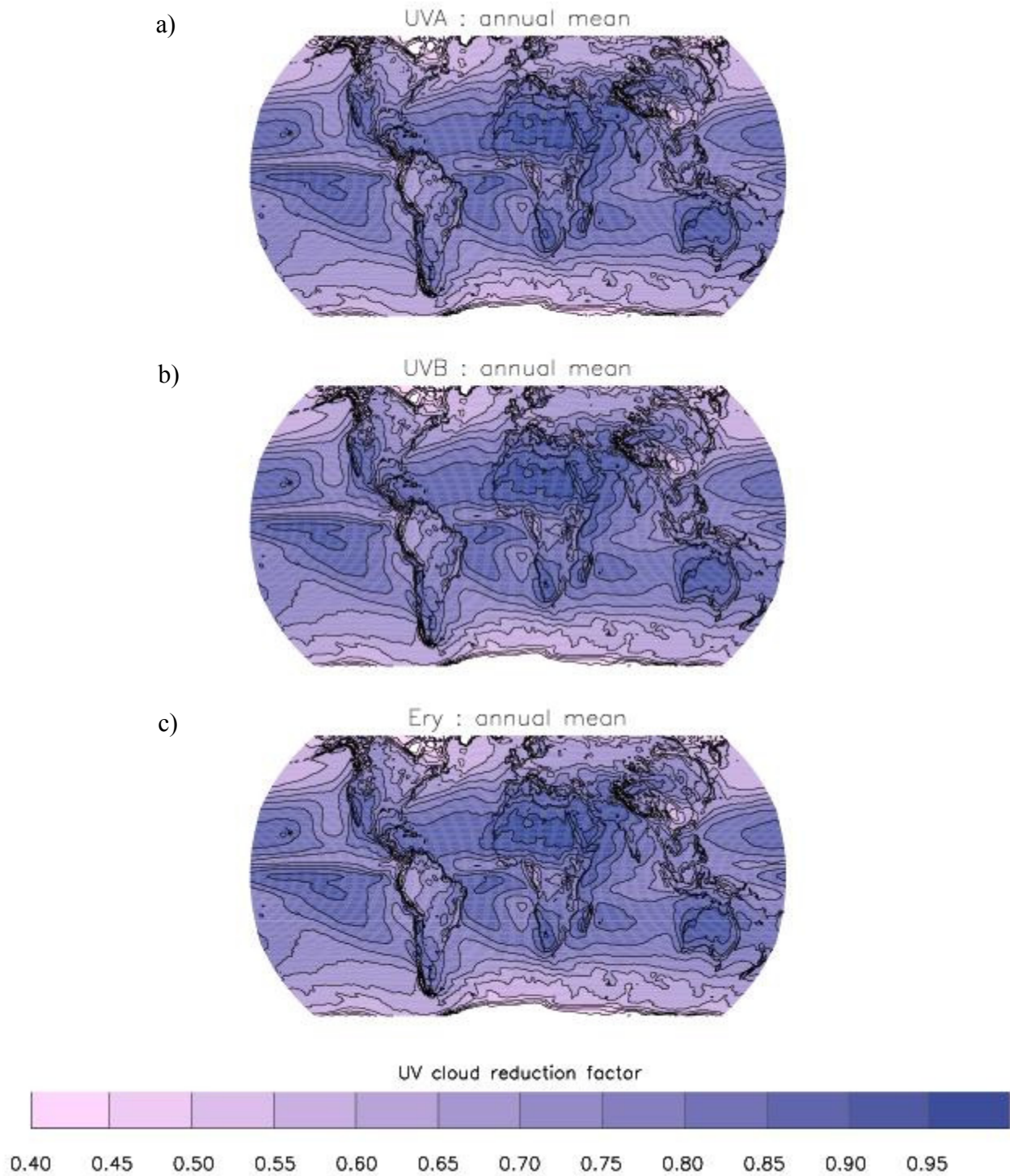


Figure 4. Climatological annual mean cloud reduction factors for daily doses of a) UV-A, b) UV-B, and c) UV_{ery} derived from satellite (TOMS) observations of the atmospheric ozone column and cloud reflectivity at 380 nm for Nov 1, 1978 – Jun 30, 2000.

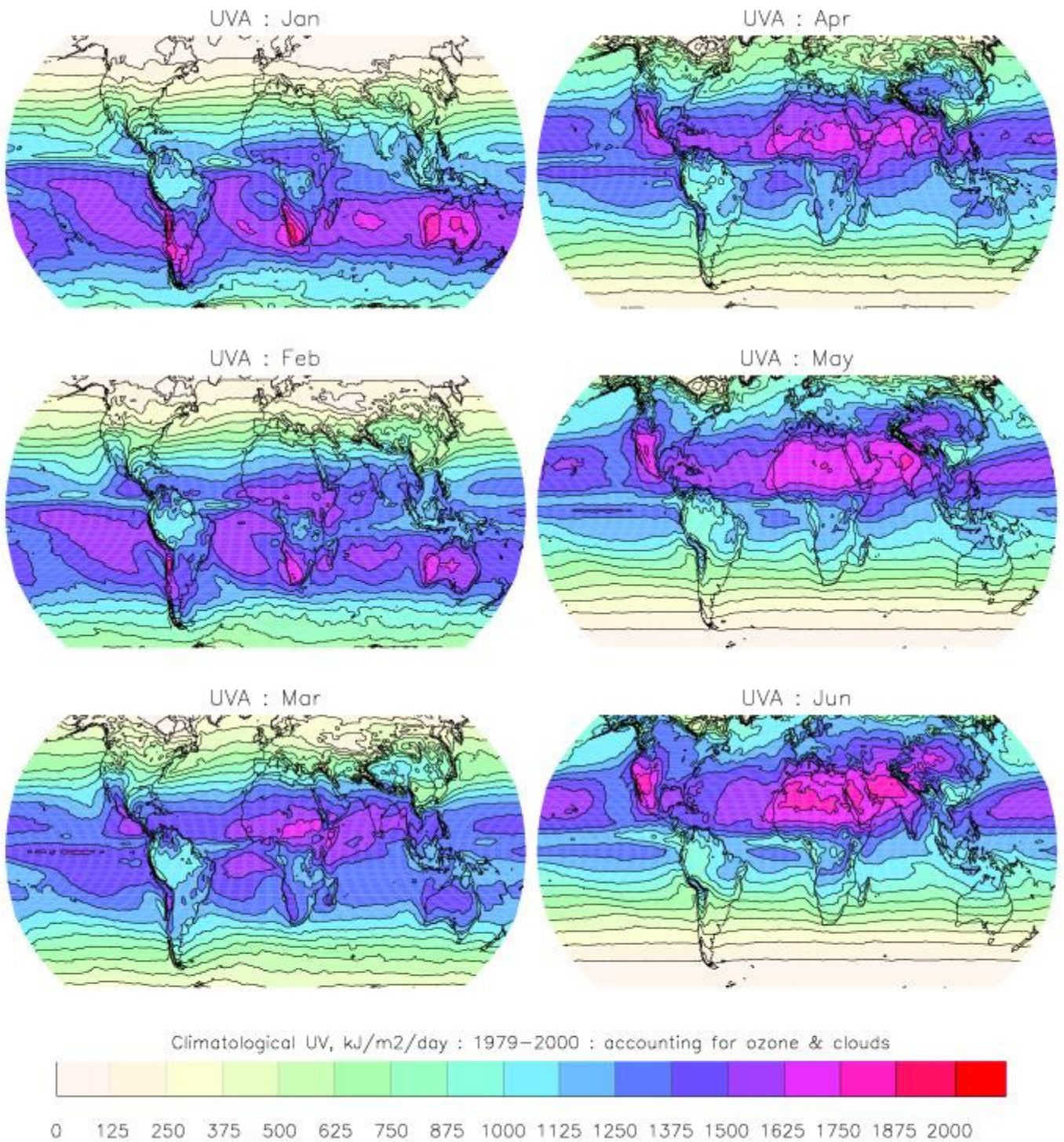


Figure 5a. Seasonal variability of daily doses of UV-A, January – June. Each panel shows the respective monthly mean of the daily doses, averaged over the period Nov 1, 1978 – Jun 30, 2000.

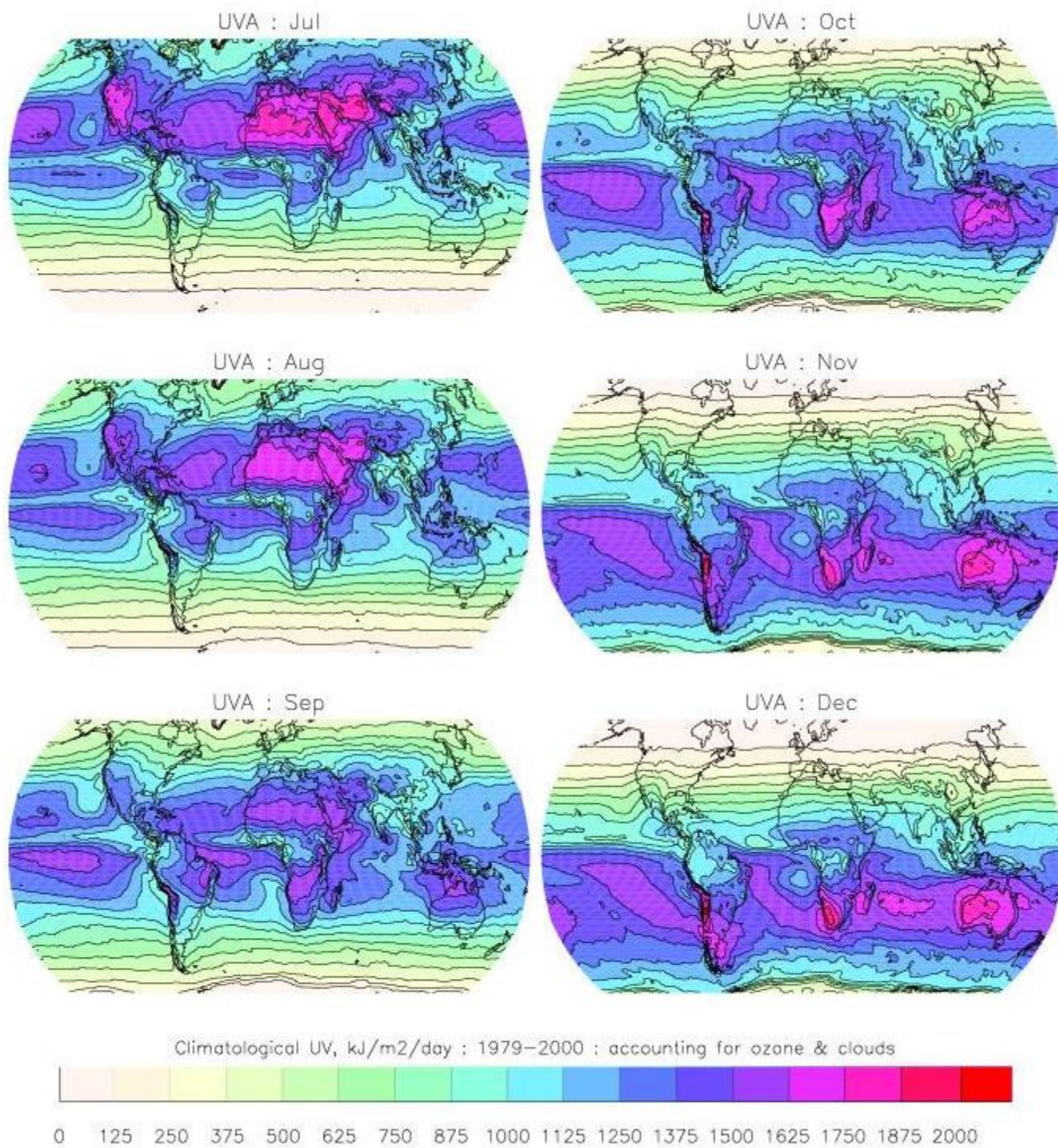


Figure 5b. Seasonal variability of daily doses of UV-A, July - December.

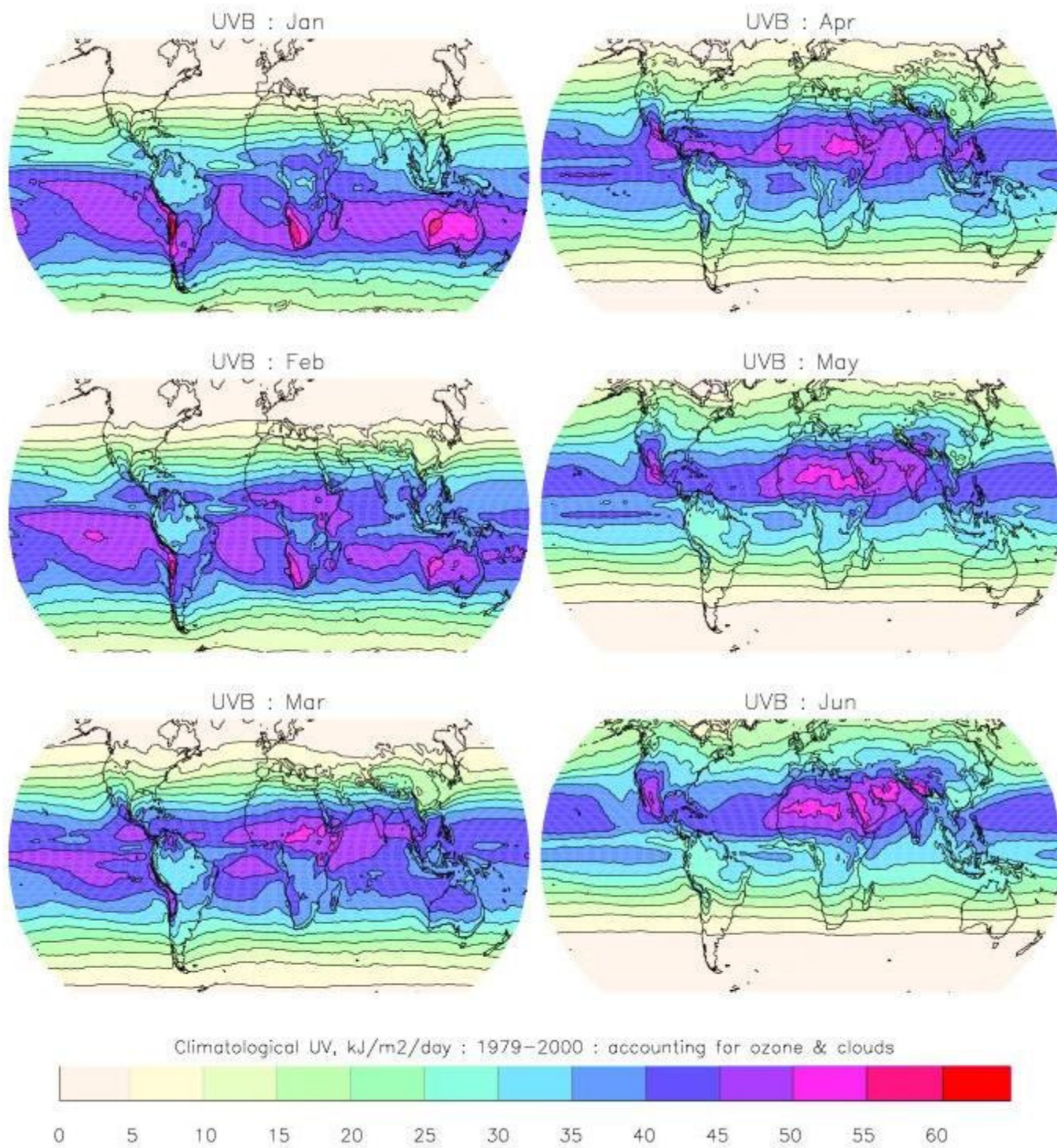


Figure 6a. As Fig. 5a, for UV-B.

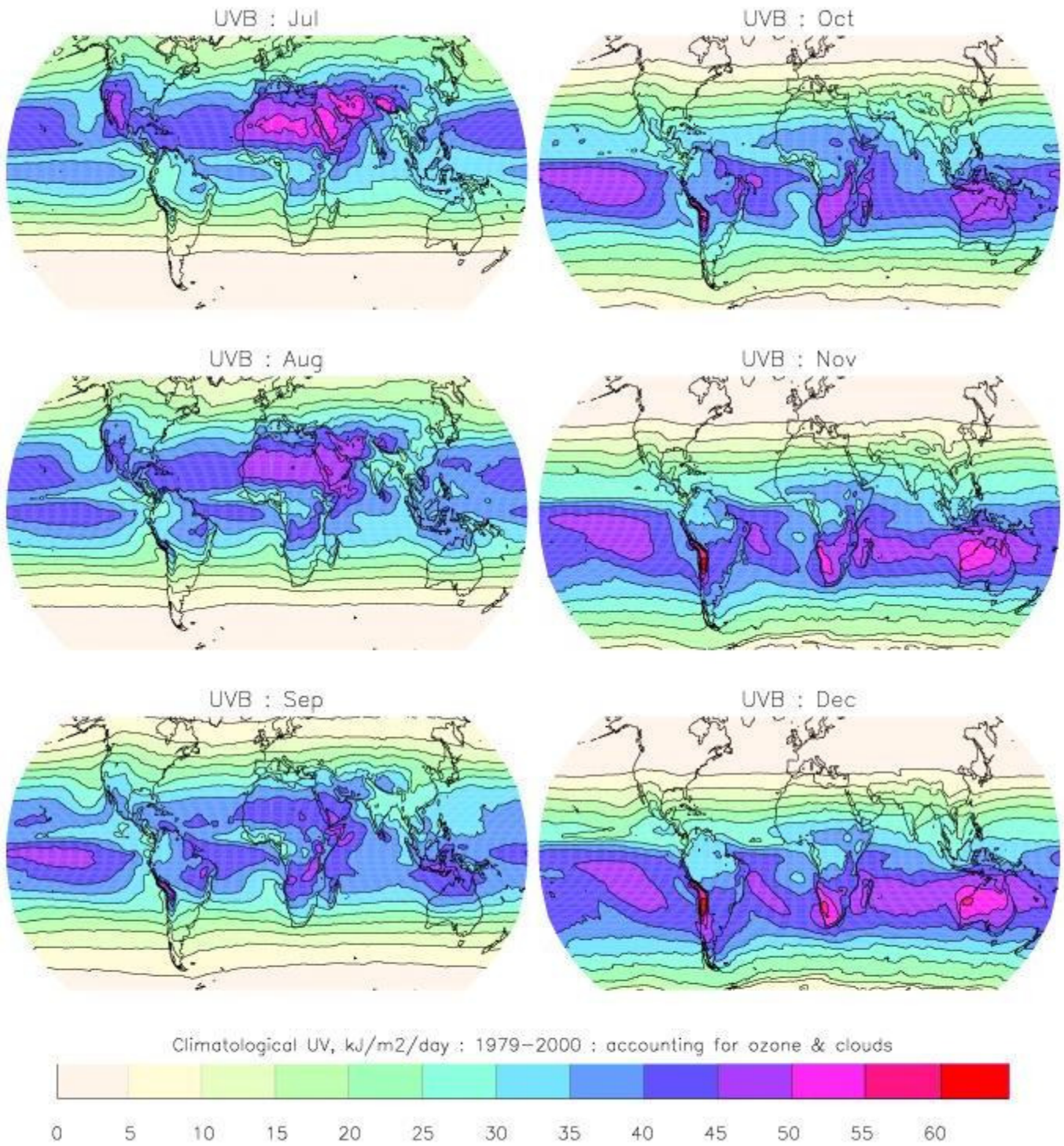


Figure 6b. As Fig. 5b, for UV-B.

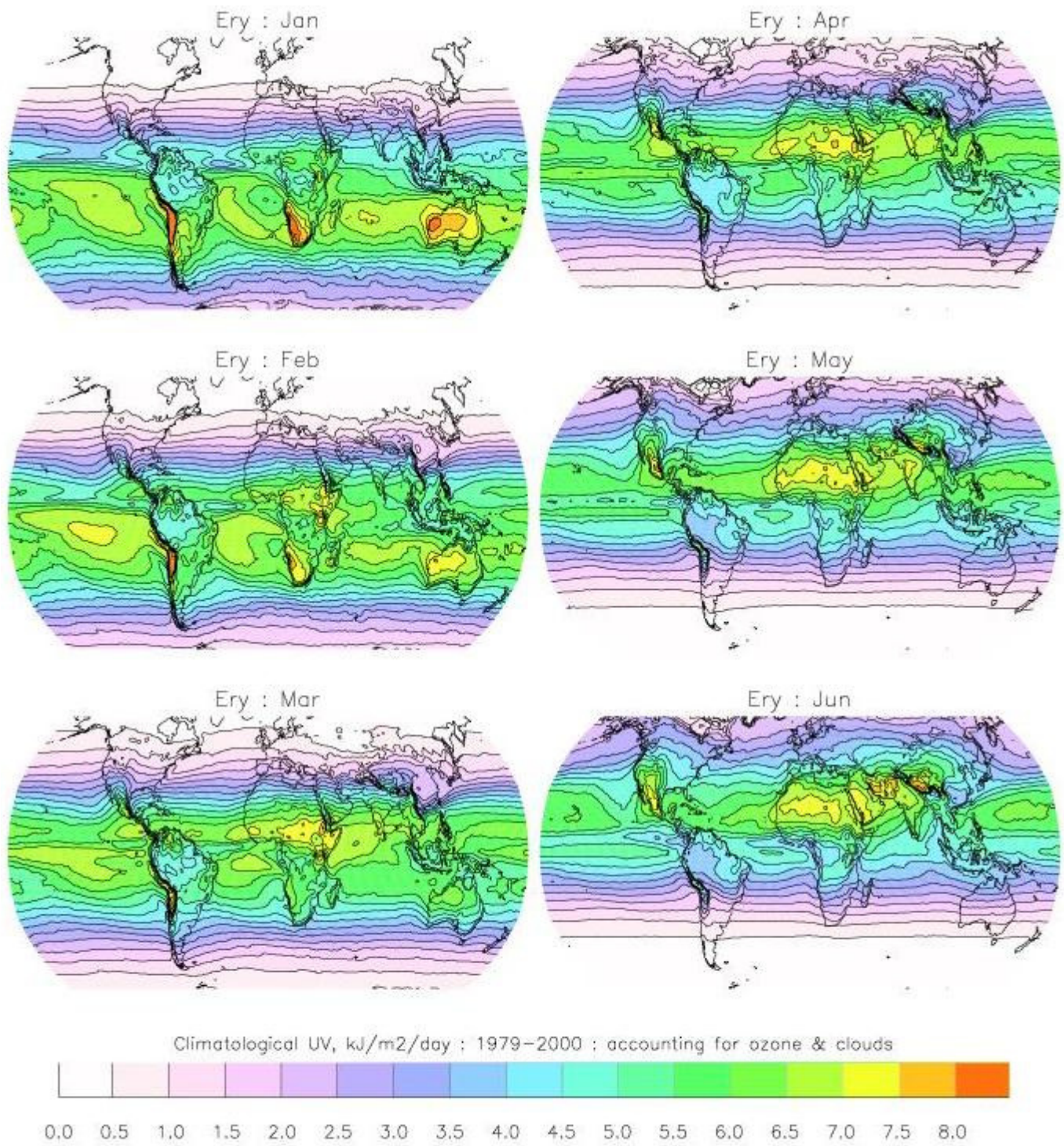


Figure 7a. As Fig. 5a, for UV_{ery}.

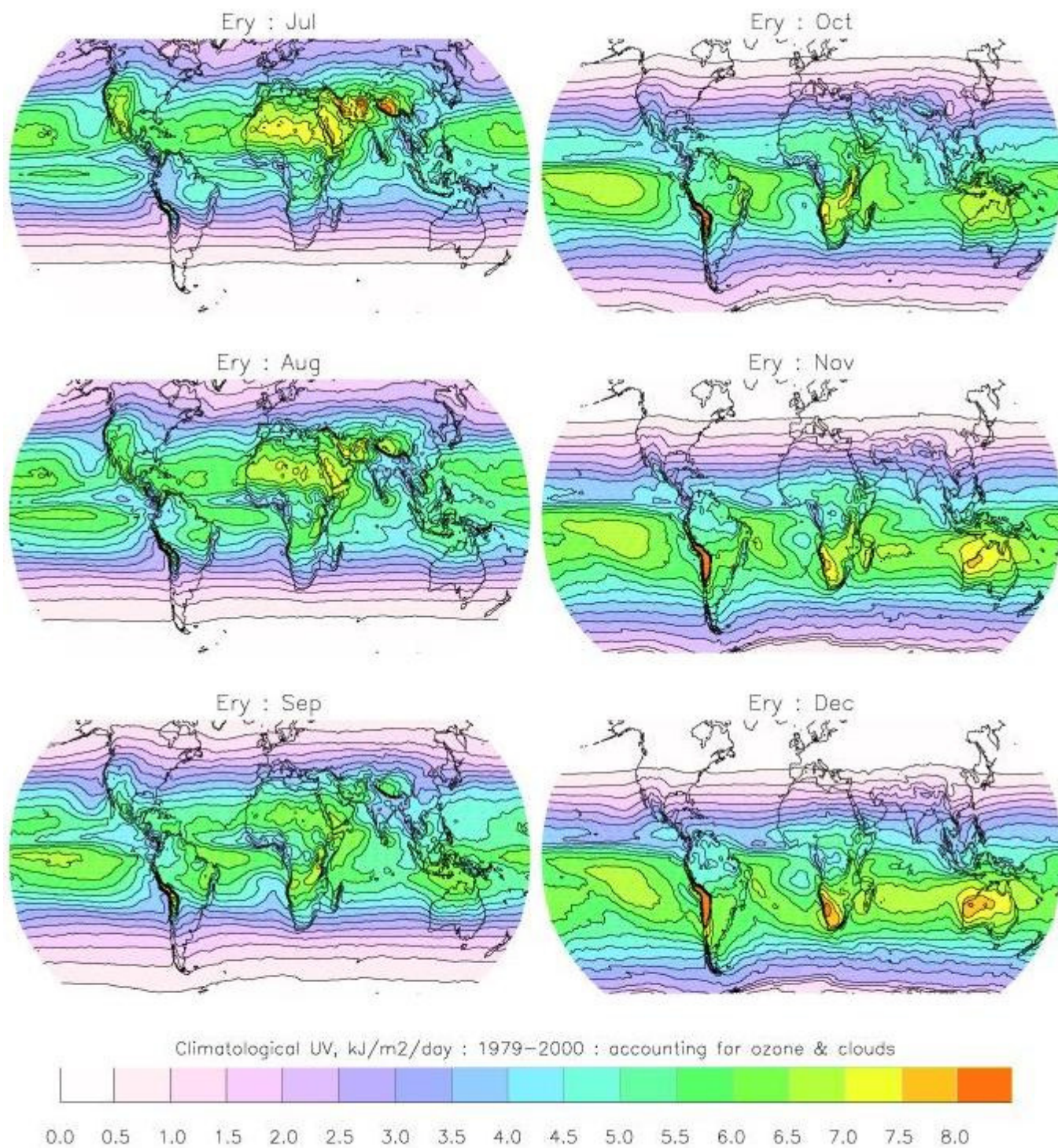


Figure 7b. As Fig. 5b, for UV_{ery} .

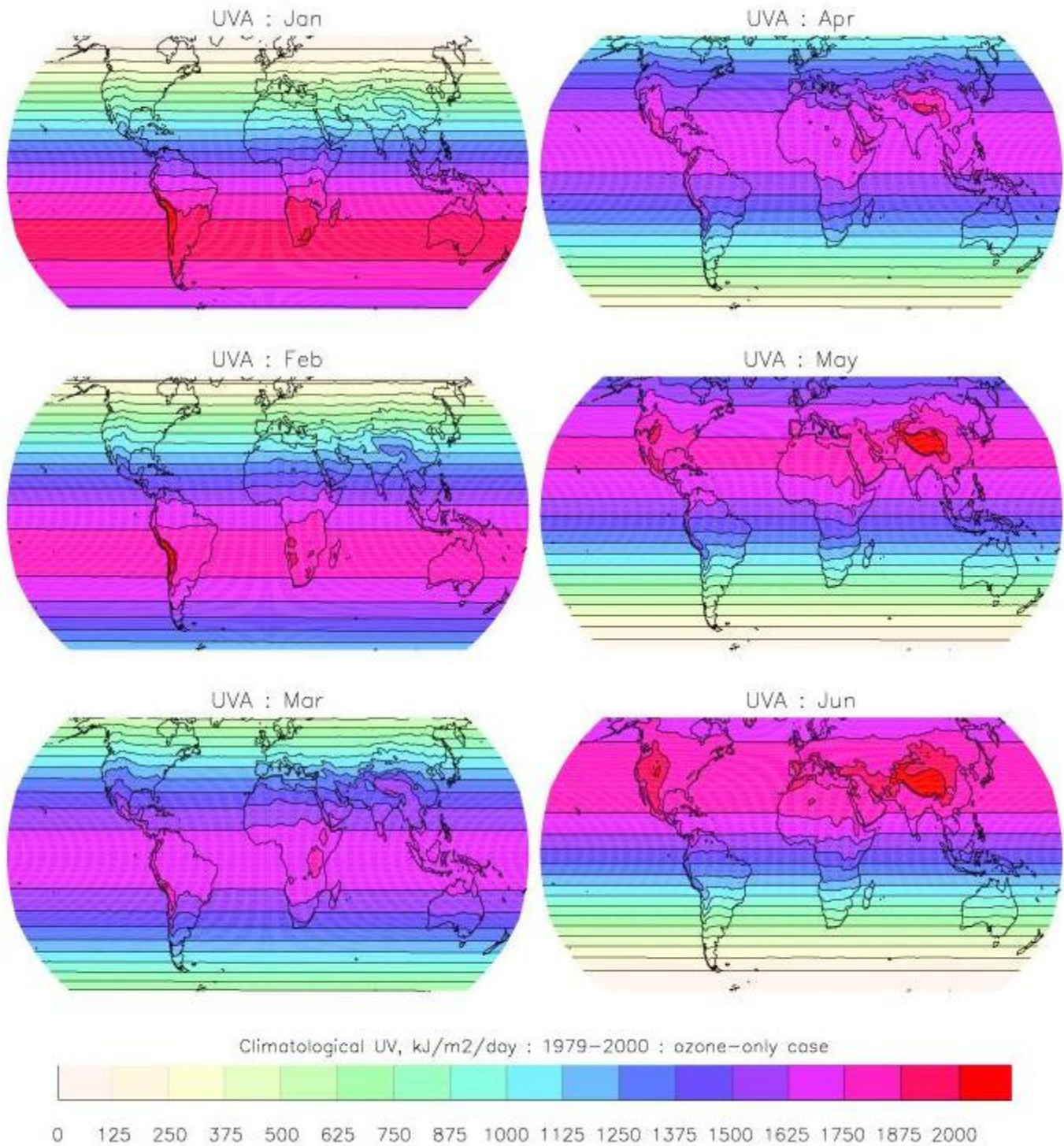


Figure 8a. Seasonal variability of UV -A calculated without correcting for the presence of clouds, January - June. Each panel shows the respective monthly mean of the daily potential doses, averaged over the period Nov 1, 1978 – Jun 30, 2000.

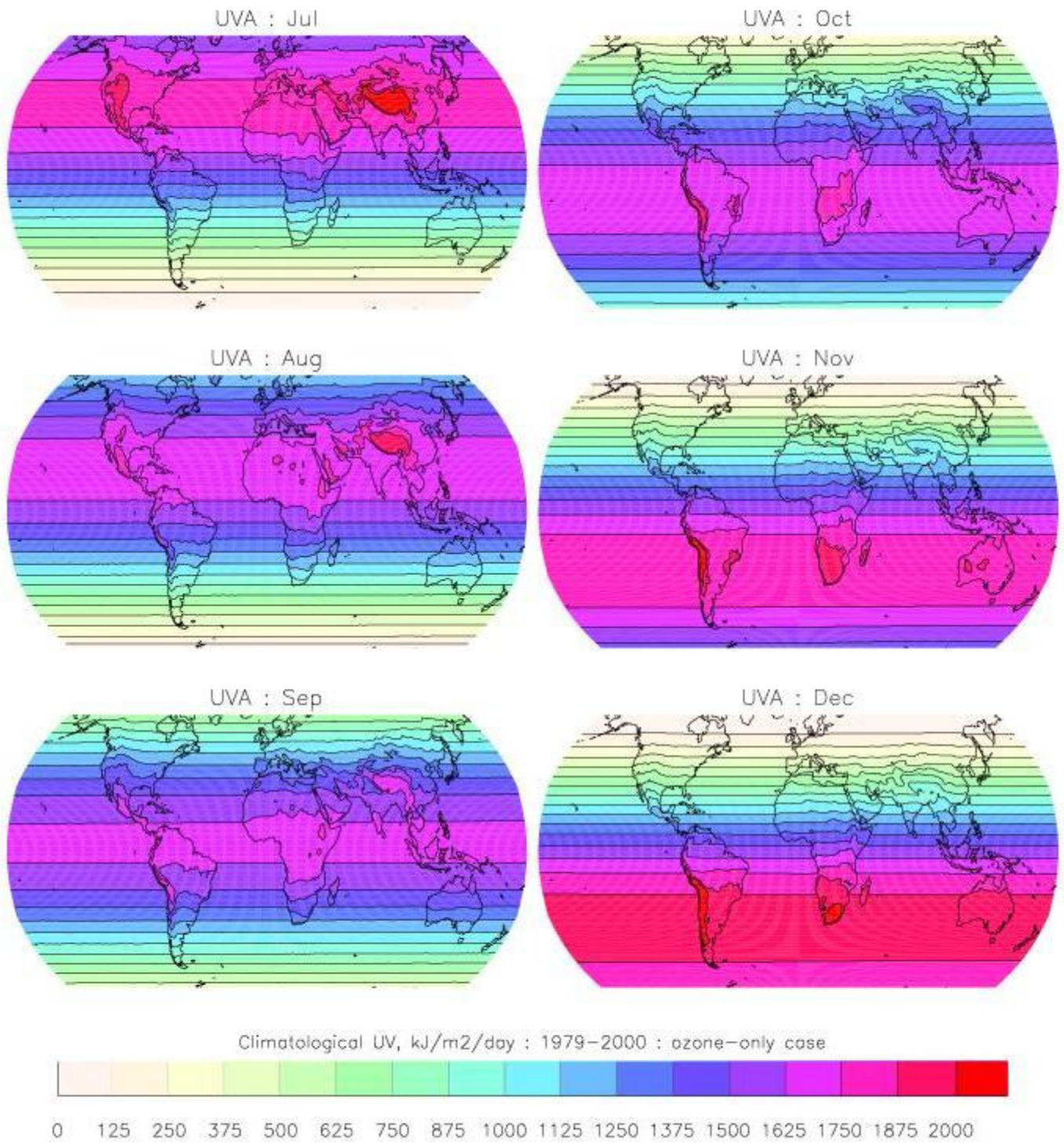


Figure 8b. Seasonal variability of UV -A calculated without correcting for the presence of clouds, July - December.

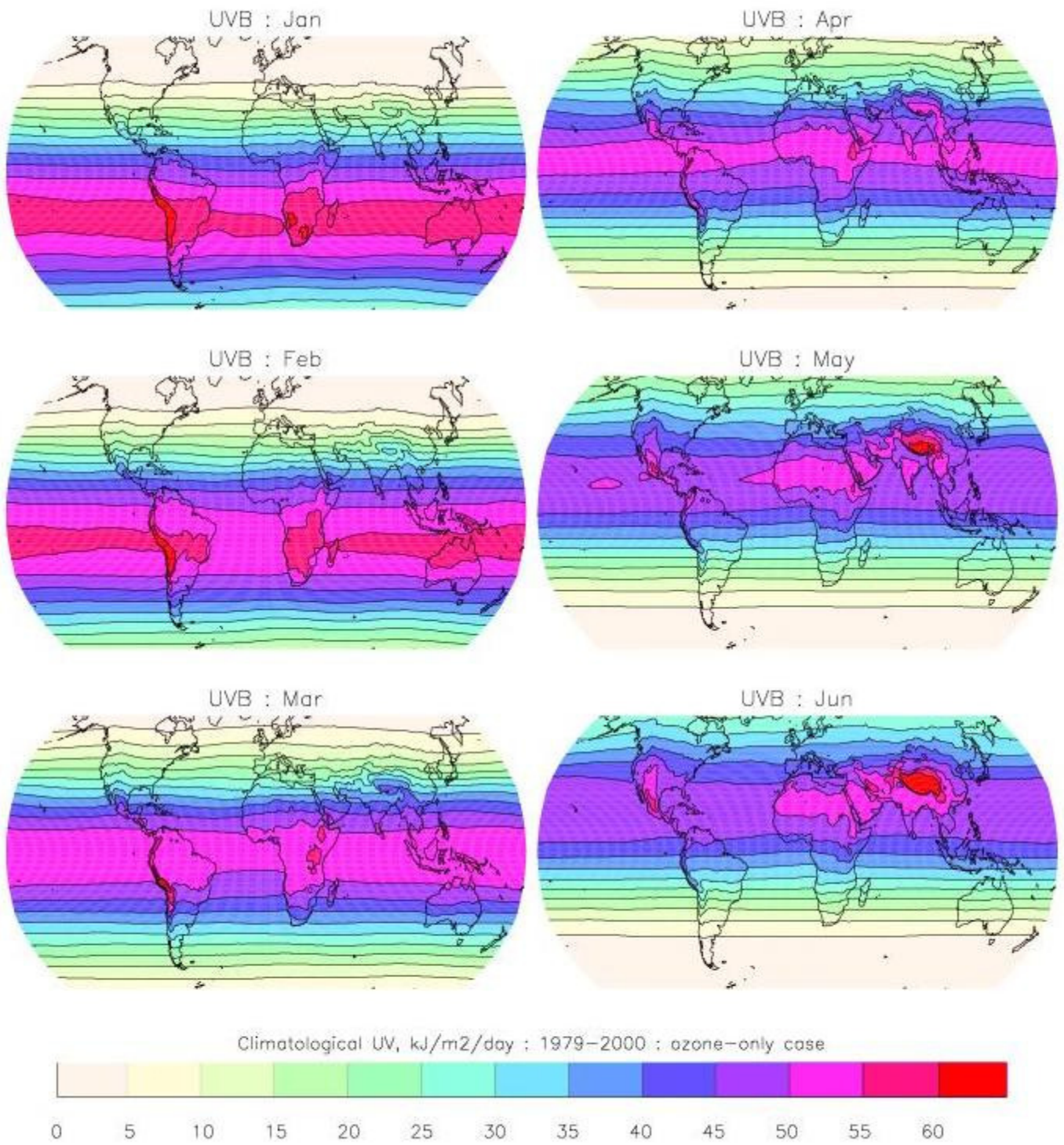


Figure 9a. As Fig. 8a, for UV -B.

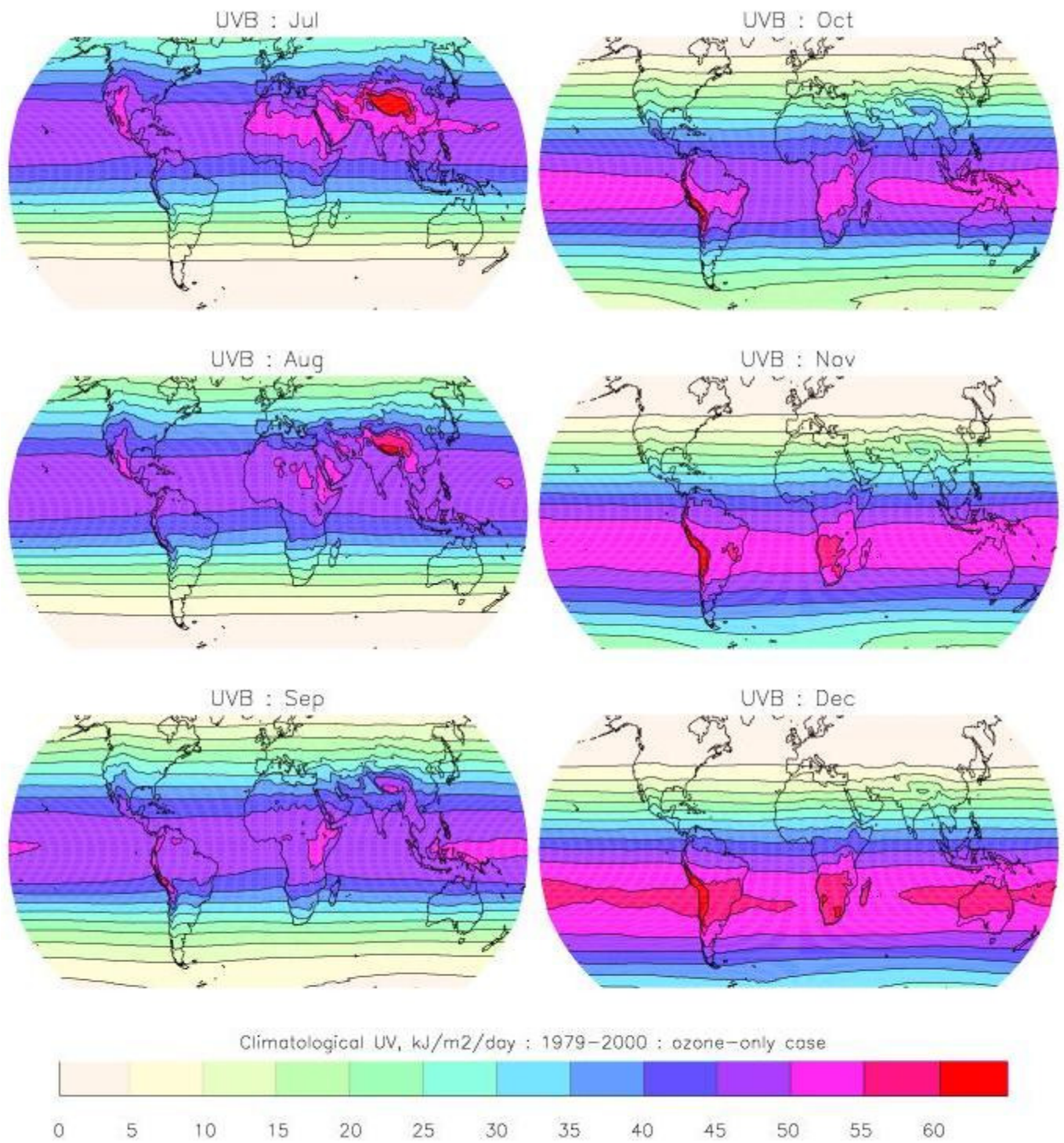


Figure 9b. As Fig. 8b for UV-B.

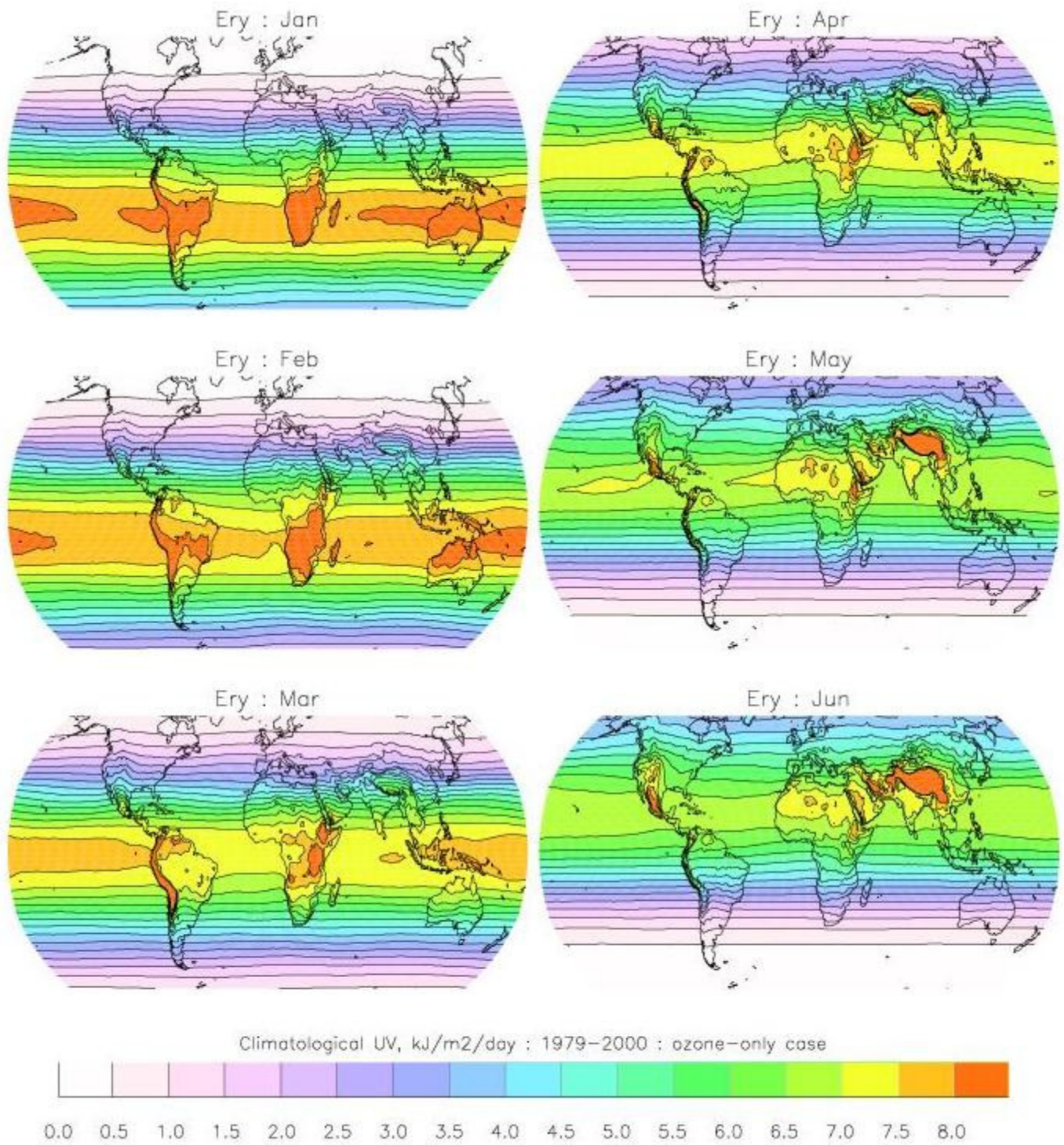


Figure 10a. As Fig. 8a, for UV_{ery} .

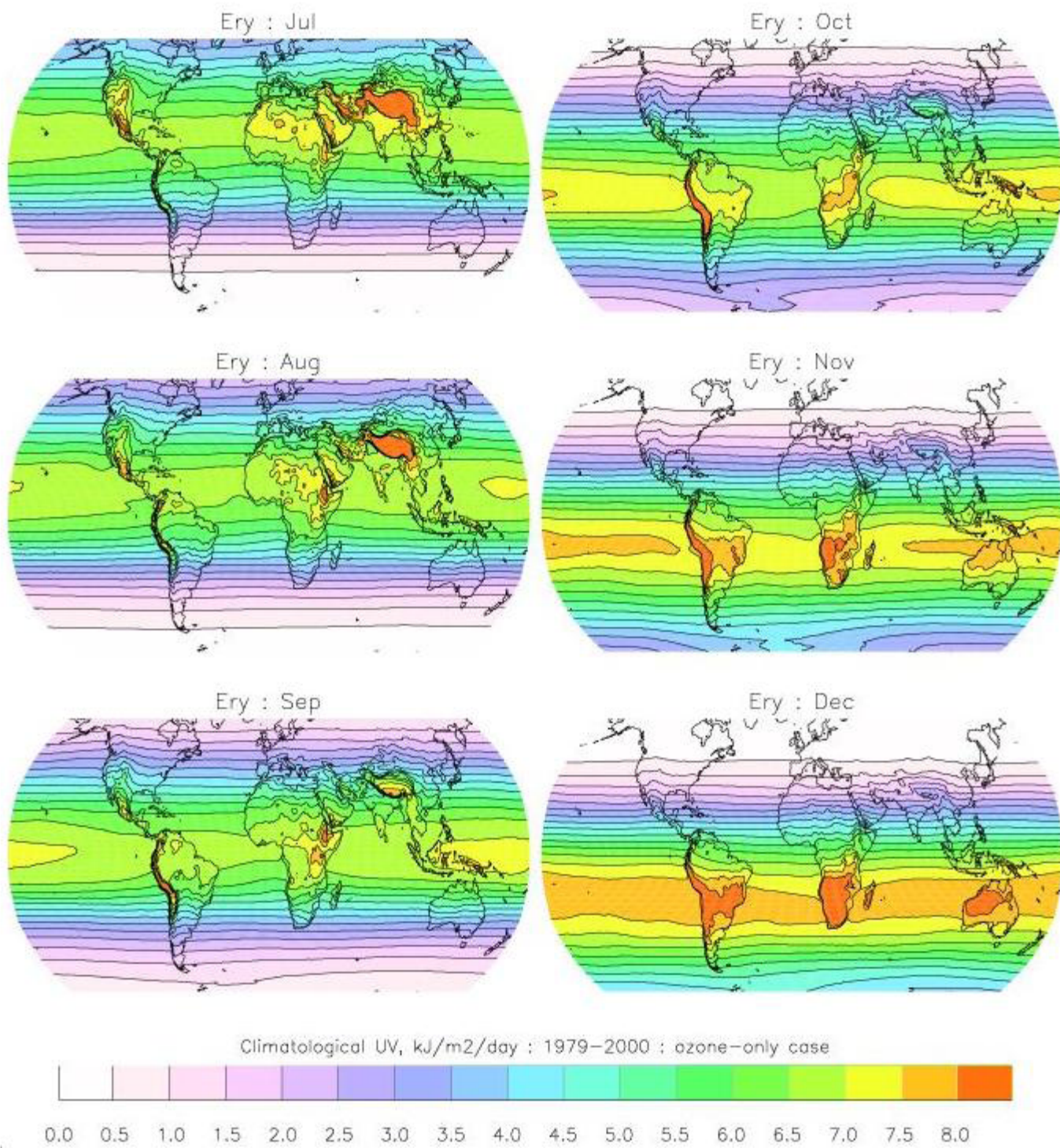
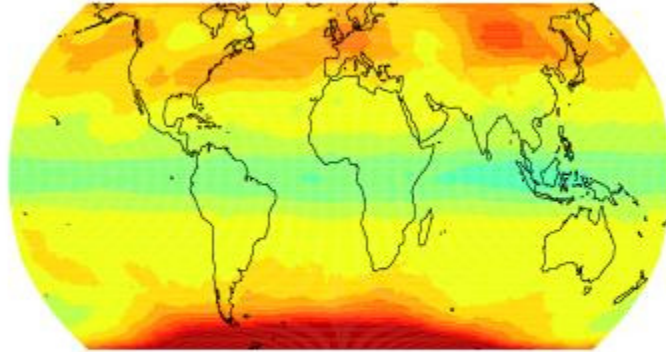
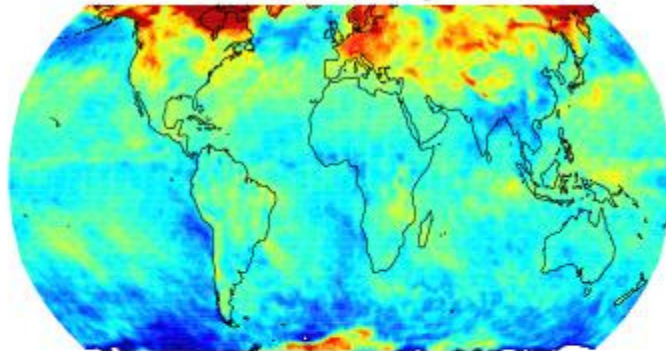


Figure 10b. As Fig. 8b, for UV_{ery} .

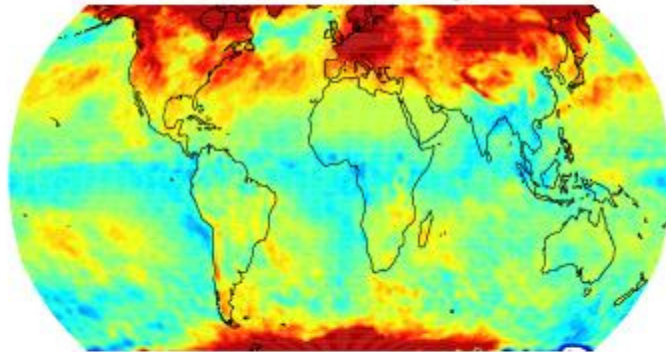
a) ERY : ozone-only case : change in annual mean



b) Cloud reduction factor : change in annual mean



c) ERY : ozone + cloud case : change in annual mean



% Change, 1980s to 1990s

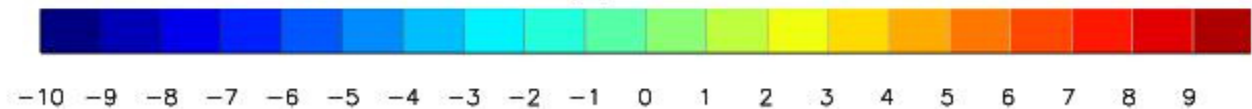


Figure 11. Changes in average daily erythemal UV doses between the periods 1979-1989 and 1990-2000. a) Change in values calculated from the TOMS ozone data only, b) change in cloud reduction factor, c) change in annual mean net daily erythemal UV dose.

3.2 Comparison with ground-based measurements

Comparisons with ground-based measurements are shown in Figure 12, for annual averages of the daily UV_{ery} dose calculated from Version 7 of the TOMS data. Temporal overlap between the satellite observations and the ground-based observations is available only at some stations, and then only for a few years. The satellite-derived estimates show a long-term trend due to stratospheric ozone depletion, as has been reported previously [Herman *et al.*, 1996], whether clouds are included or not. Note that the satellite-derived values apply to an extended region of typically 10^4 km^2 , while the ground-based observations pertain to a single, often urban, location. Figure 13 shows that our satellite-derived annual averages tend to overestimate measurements by averages of 5% for remote northern locations, 11% for Canadian cities, and 30% for polluted midlatitude urban regions (San Diego and cities in Japan and Taiwan). Herman *et al.* [1999] found similar differences for the measurements at Toronto, showing also that these were not seasonally dependent except for snow-covered periods. These discrepancies remain under investigation and may stem from both measurements and satellite-derived values. Because of the imperfect cosine response of the entrance optics, Brewer instruments may underestimate true irradiances by 2-7% according to Bais *et al.* [1998], or by $6 \pm 2\%$ according to Herman *et al.* [1999]. The TOMS-based method does not account for UV-absorbing aerosols, which according to Herman *et al.* [1999] lead to a systematic overestimate of ca. $8 \pm 2\%$ at Toronto. Aerosols are likely to be significant at other locations during pollution episodes [e.g., Wenny *et al.*, 1998], or if an area suffers routinely from pollution (e.g. the south-east Asian sites). Smaller errors (e.g. 5% or less) are associated with several other factors (e.g. instrument calibrations, extraterrestrial irradiances used in the model) but at present there is no basis for estimating the sign of any resulting bias. The strong disagreement at Palmer station, where we underestimate the irradiance by 50%, illustrates the consequence of using TOMS-observed reflectivity to infer cloudiness at high-latitude locations. The high reflectivity recorded by the satellite may be due to snow and ice rather than to clouds, thus leading to a significant underestimate of the UV_{ery} reaching the surface.

Using a similar TOMS-based technique, Frederick and Erlick [1995] computed noon-time erythemal irradiances, as well as their trends and interannual variability, for regions of 6° latitude by 10° longitude centered over New Zealand, Malaysia, Sweden and the eastern United States. Lubin *et al.* [1998] used monthly mean ozone from TOMS and monthly mean cloud cover data derived from ERBE (Earth Radiation Budget Experiment) to compute global UV_{ery} distributions for several months of 1988 and 1989. Sabziparvar *et al.* [1999] presented a global climatology of daily doses for January, April, July, and October, computed from monthly-averaged climatological ozone (TOMS, 1985-1989) and cloud data (International Satellite Cloud Climatology Project, ISCCP, 1983-1991). Global distributions of UV_{ery} for 1988 (January, March, July, and September) are presented by Herman *et al.* [1999], who also carried out detailed comparisons to observations obtained with the Toronto Brewer instrument. Our results are generally consistent with these studies, for example in predicting the strong latitudinal gradients as well as most of the local anomalies. Detailed values are however not directly comparable because of our use of daily rather than monthly ozone and cloud data, and our integration over an extended time period (1978-2000).

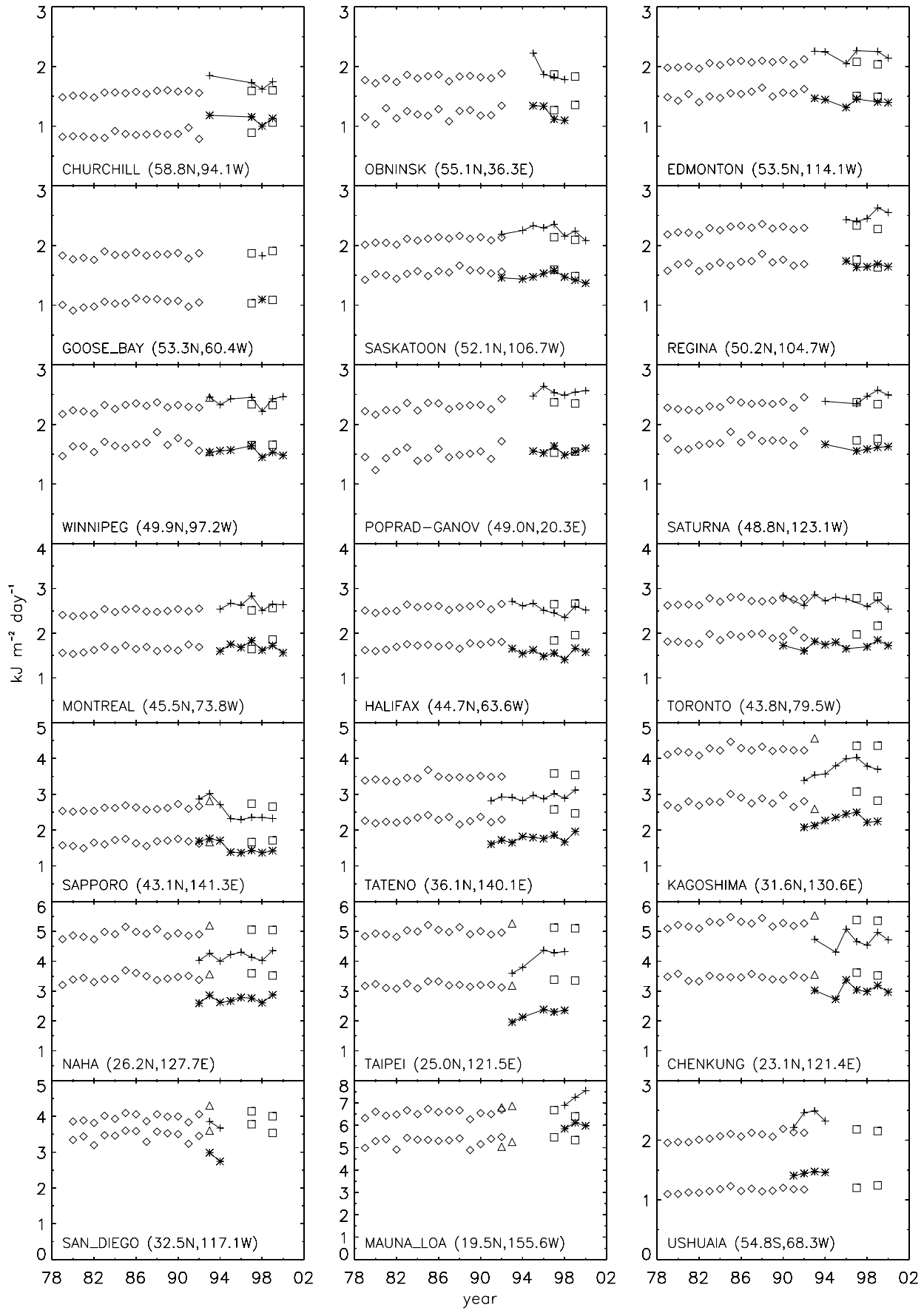


Figure 12 (previous page). Comparison of yearly-averaged daily erythemal UV doses derived from satellite observations with those derived from ground-based measurements at 21 stations. Open symbols, satellite-derived values with (lower) and without (upper) adjustment for the presence of clouds: diamonds, Nimbus-7; triangles, Meteor-3; squares, Earth Probe. Plus signs, annual mean of monthly maximum measurements; stars, annual mean of monthly mean measurements. In all averaged cases, yearly means are shown only for datasets containing 12 valid months, defined as months where data is present for more than half of the days in the month. See Table 1 for station details.

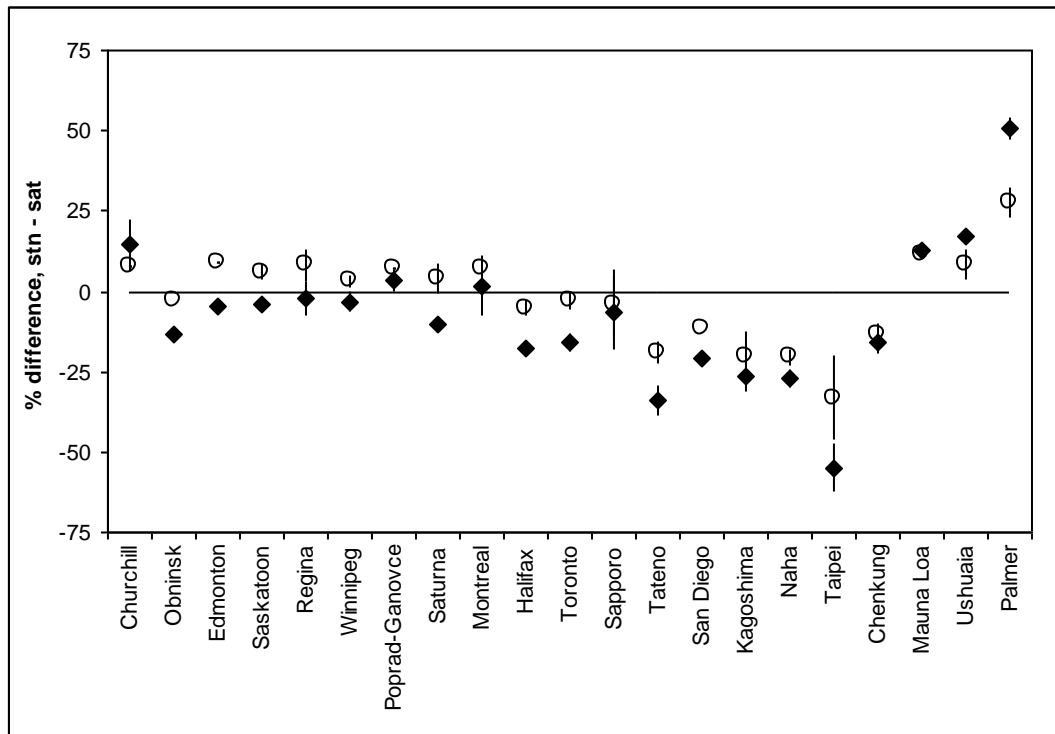


Figure 13. Differences between ground-based and satellite-derived annual mean daily erythemal UV doses. Points show the mean of differences for all years where both ground-based and satellite-derived values are available. Lines show the standard deviations at each station. Filled diamonds, satellite-derived UV values including adjustment for the presence of clouds, and mean ground-based values; open circles, satellite-derived UV values without cloud adjustment, and maximum ground-based values. Stations are listed in order of decreasing latitude. See Table 1 for station details.

5 CONCLUSIONS

We recognize a number of limitations in our study that can hopefully be addressed by future work. The parameterization of cloud effects via the 380 nm reflectivity is obviously crude compared to the complexity of real cloudiness, and its failure in the presence of high albedo surfaces has been discussed. Other sources of cloud information exist and show promise in extending the climatology to higher latitudes [e.g., *Mayer and Madronich, 1998*]. Also, pollutants present in the lower atmosphere can attenuate surface UV irradiances. Regional-scale absorbing aerosols, probably associated with plumes of biomass burning, have been detected by the TOMS instrument [*Krotkov et al., 1998*], although quantification remains a challenging area of research. On smaller scales, such as highly polluted urban areas, substantial absorption of UV radiation is possible from smog-generated ozone, SO₂, NO₂, and absorbing aerosols (e.g., soot) in the lower atmosphere. These absorbers are not easily detected from satellite platforms, so that a climatology based on direct ground-based UV radiation measurements, if available, is preferable for such locations.

The results shown here do not give the short-term variations in UV_{ery} although some of the inter-annual variability may be inferred from Figure 14. Daily data (1979-94 and 1996-2000) are available and were used to compute the long-term averages, but space limitations preclude their presentation here.

The climatology (Fig. 10) is potentially useful for the study of effects of long-term exposure, especially if geographical gradients are of interest. For example, the induction of non-melanoma skin cancers is now thought to be associated with long-term cumulative exposure to UV radiation [e.g., *UNEP, 1998*], hence Figure 10 and the associated data files may be of direct utility to related epidemiological studies.

ACKNOWLEDGEMENTS

The authors would like to thank Bernhard Mayer and Chris Fischer for development work that contributed to this study. This work was supported by the Department of Energy through grant DE-A105-94ER61879 to NCAR. The National Center for Atmospheric Research is operated by the University Corporation for Atmospheric Research under sponsorship of the National Science Foundation.

APPENDIX A. ADDITIONAL UV WEIGHTING FUNCTIONS

Two additional distributions of weighted UV radiation were calculated using the methods described previously. The action spectrum for previtamin D₃ production in human skin was presented by Holick *et al.* (2006), after MacLaughlin *et al.* (1982), while the action spectrum for photocarcinogenesis of non-melanoma skin cancers was published by CIE (2006). The functions are somewhat similar, in that they maximise at around 300 nm wavelength, and drop sharply within 20 nm either side of the peak.

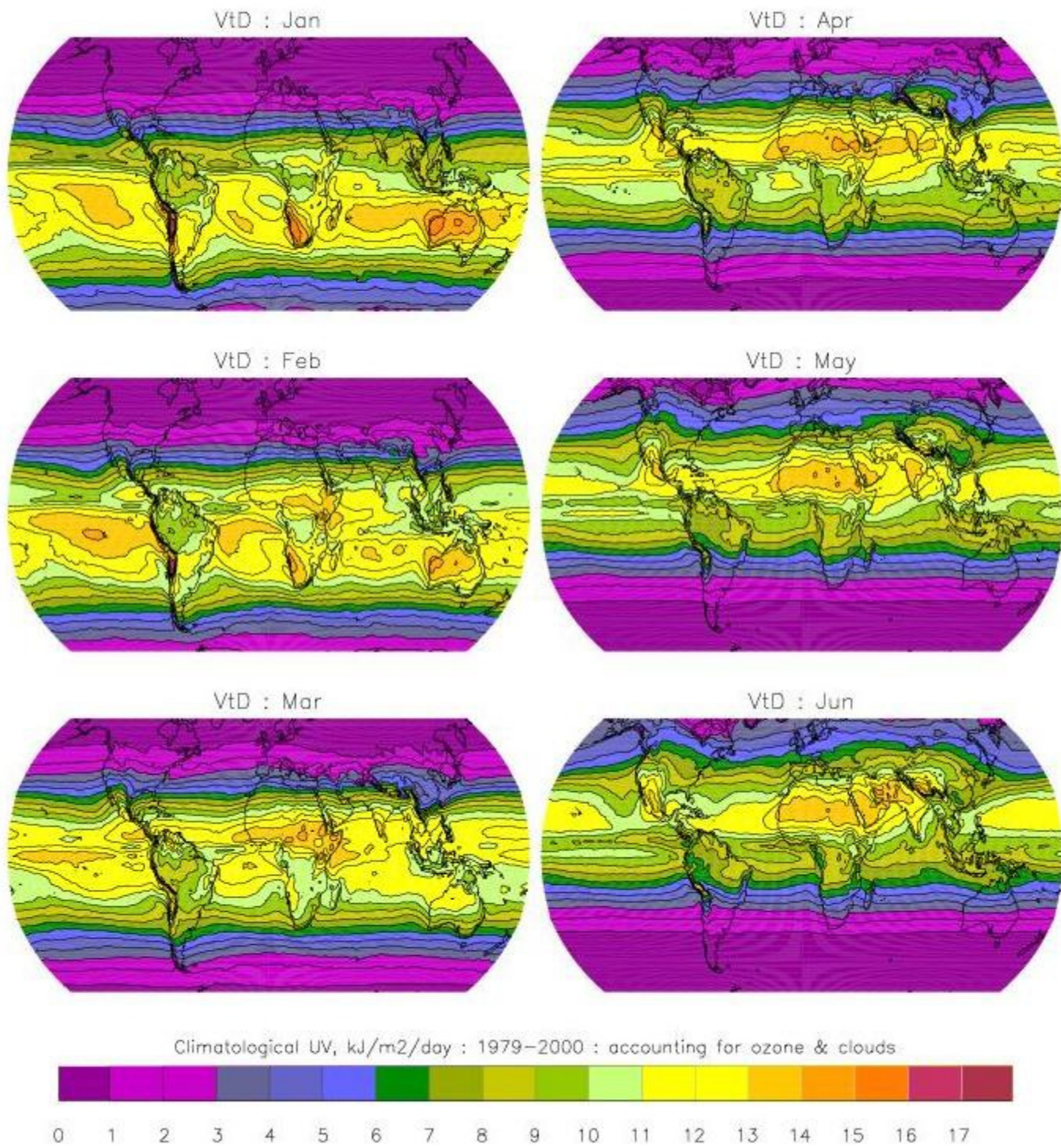


Figure A1a. Seasonal variability of UV weighted for previtamin D3 production in human skin, January - June. Each panel shows the respective monthly mean of the daily potential doses, averaged over the period Nov 1, 1978 – Jun 30, 2000.

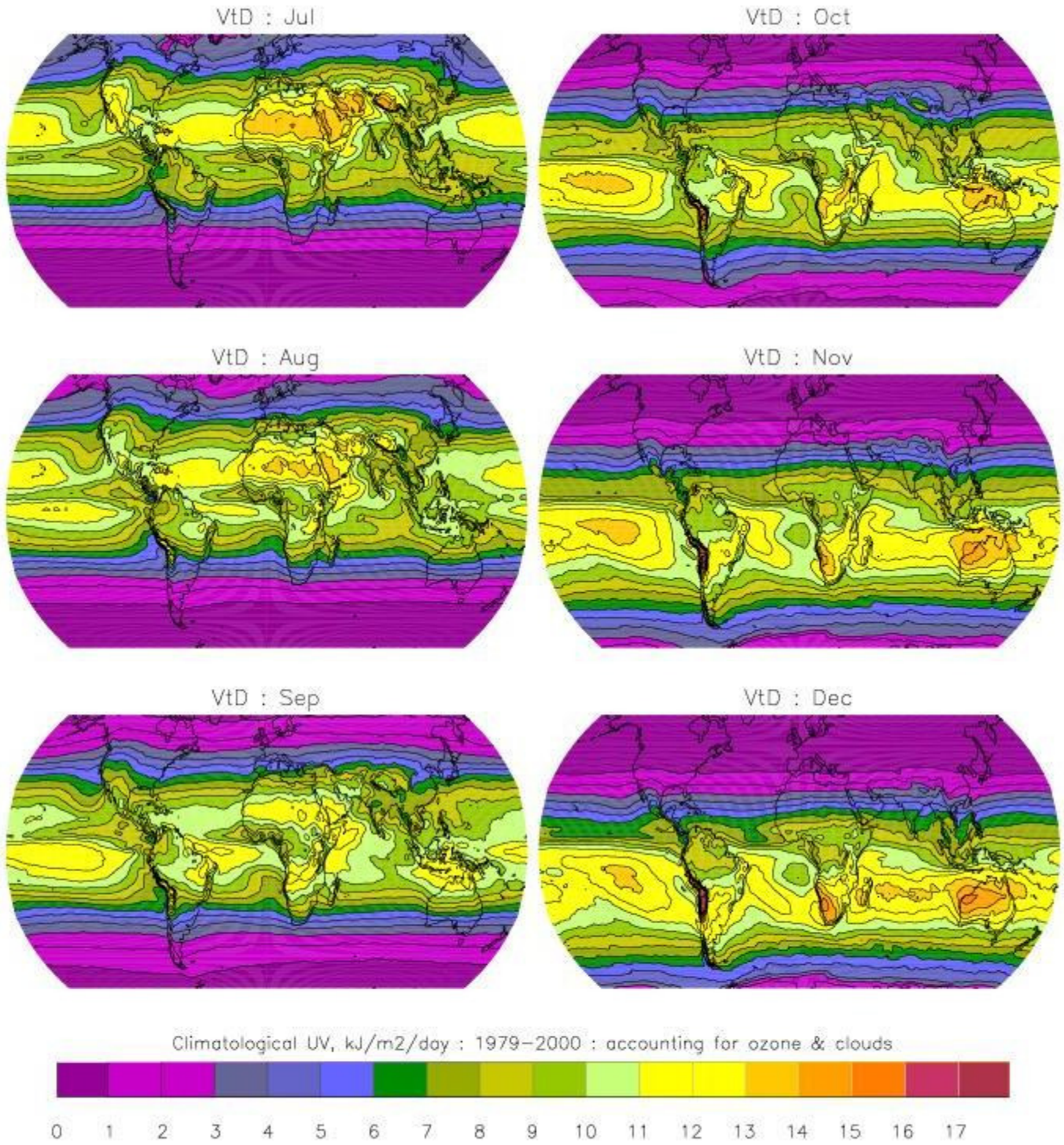


Figure A1b. As Fig. A1a, for July – December.

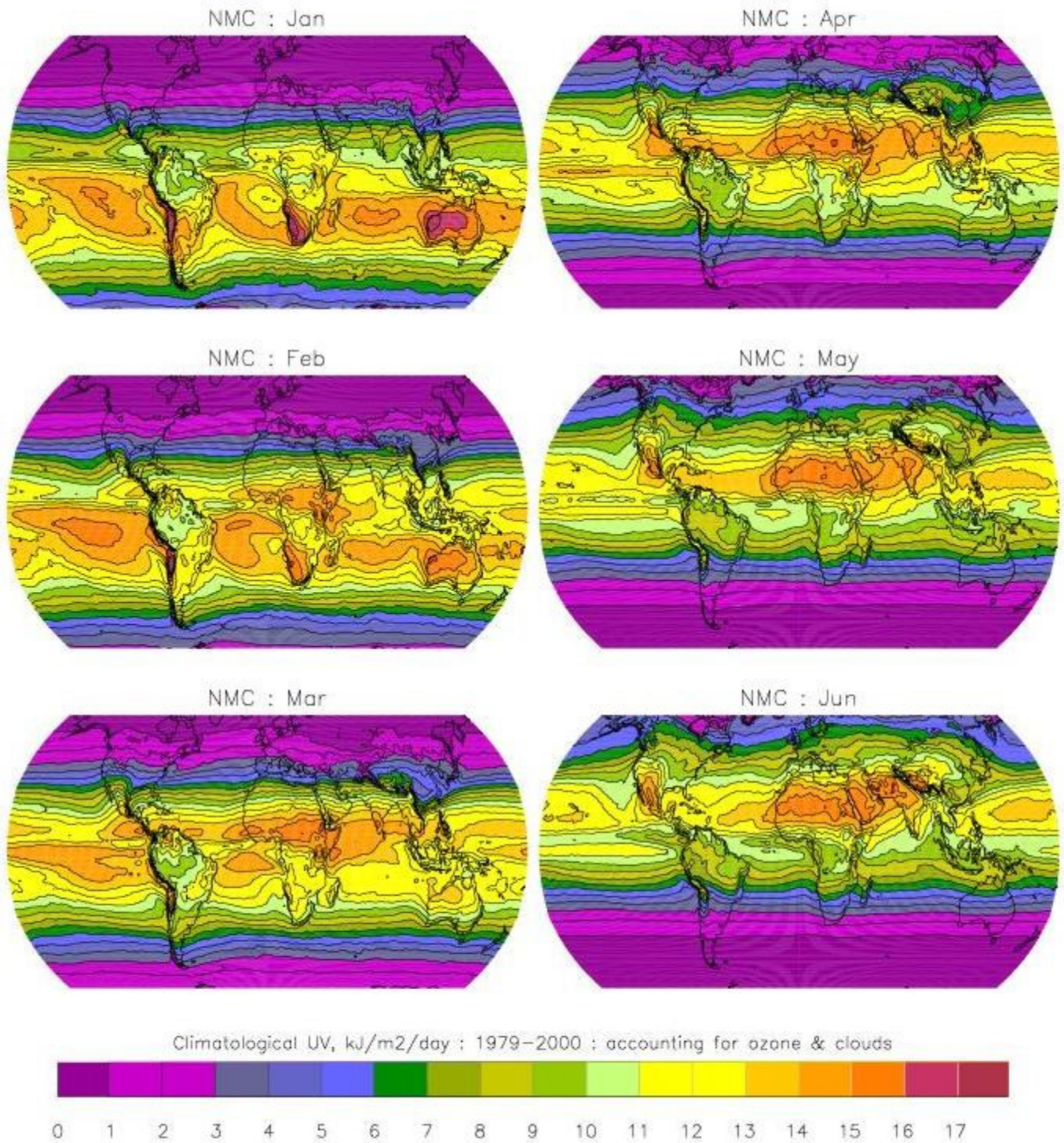


Figure A2a. Seasonal variability of UV weighted for non-melanoma carcinogenesis in human skin, January - June. Each panel shows the respective monthly mean of the daily potential doses, averaged over the period Nov 1, 1978 – Jun 30, 2000.

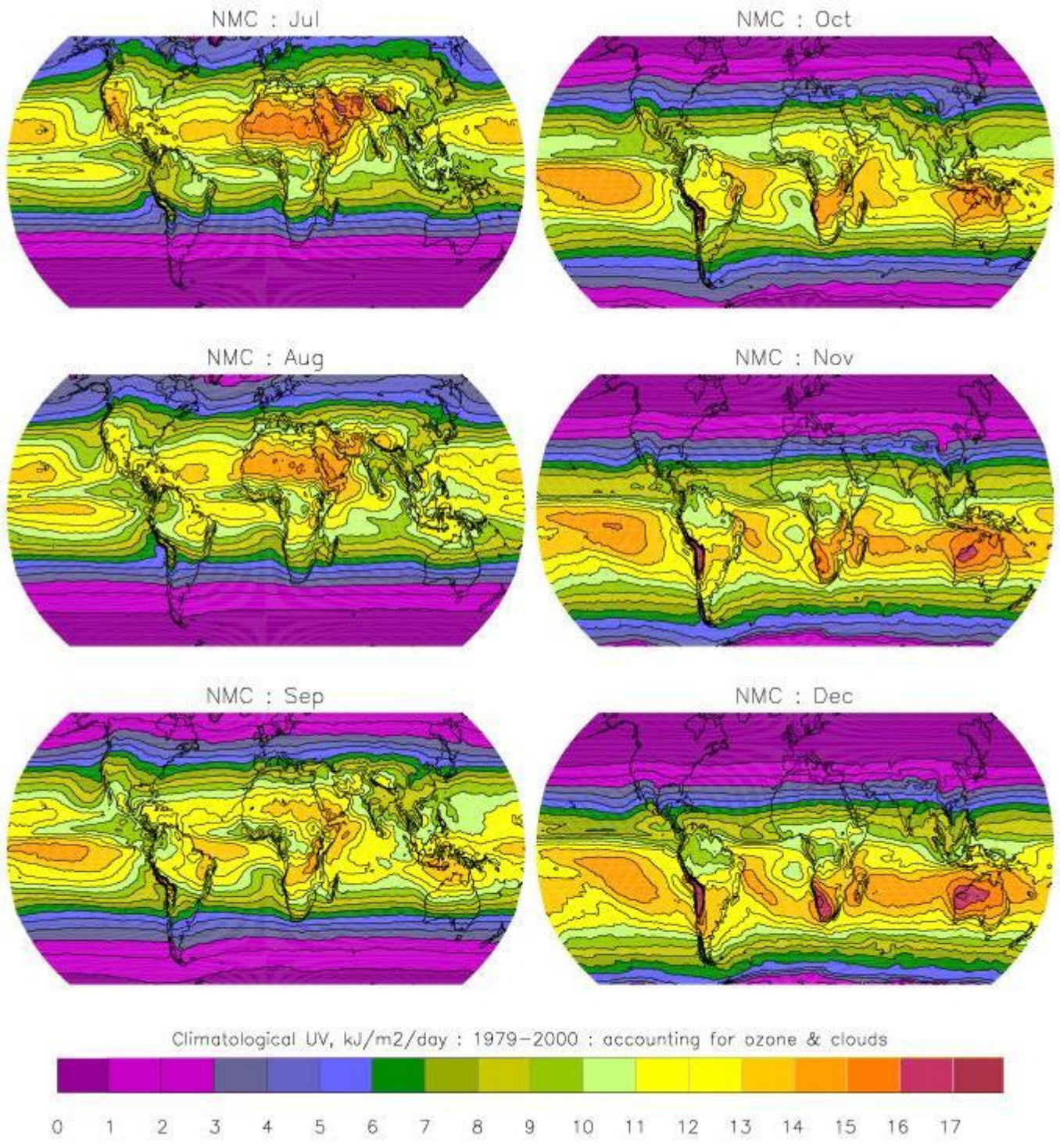


Figure A2b. As Fig. A2a, for July – December.

APPENDIX B. DATASETS AVAILABLE FOR DOWNLOAD

The weighted UV distributions described in this Technical Note are available for free download from the NCAR Community Data Portal, at: <http://cdp.ucar.edu>

To find the datasets, navigate the ‘browse’ menu through the directory structure:

ACD > ACD Models > TUV > Erythema_UV

First-time users are required to create a login.

Climatologies are available for the periods 1979-1989, 1990-2000, and 1979-2000. The 1979-2000 climatology of erythema UV is also available for download as a postscript figure.

Download filenames are of the form *clim_y1-y2.name.zip* where *y1* and *y2* are the last two digits of the first and last years of the climatology, respectively, and *name* is the three-letter abbreviation assigned to the weighting function (see Table A1). Monthly filenames are of the form *y1y2mm.name.dat* where *mm* is the month, and *y1*, *y2*, and *name* are as already defined.

Each download file contains twelve ascii files (for months January through December). Figure A1 shows the first six lines of a sample data file, including the three-line header. Total UV irradiance values are given in units of kJ/m²/month for ozone-only calculations, and for climatological cloudiness. The data are arranged by longitude and latitude, starting at the South Pole dateline and progressing east and then north.

Table B1. Abbreviations for spectral weighting function names

<i>name</i>	Weighting Name	Spectral Range	Reference
UVA	UV-a	315-400 nm	
UVB	UV-b	280-315nm	
Ery	human erythema	250-400nm	McKinlay & Diffey, 1987
VtD	previtamin D ₃ production	252-330nm	Holick <i>et al.</i> , 2006; MacLaughlin <i>et al.</i> , 1982
NMC	photocarcinogenesis (non-melanoma skin cancers)	250-400nm	CIE, 2006

Figure B1. Example data file

units: kJ.m-2.month-1

11-year climatological monthly means, 1979-1989, month = 1

lat long ozone-only ozone+cloud

-89.5 -179.375 5.501e+04 5.042e+03

-89.5 -178.125 5.501e+04 5.042e+03

-89.5 -176.875 5.501e+04 5.042e+03

(etc...)

REFERENCES

- Bais, A., S. Kazadzis, D. Balis, C. Zerefos, and M. Blumthaler, Correcting global solar ultraviolet spectra recorded by a Brewer spectroradiometer for its angular response error, *Appl. Optics*, 37, 6339-6344, 1998.
- CIE (Commission Internationale de l'Eclairage), Erythema Reference Action Spectrum and Standard Erythema Dose, CIE S 007/E-1998, Vienna, 1998.
- CIE (Commission Internationale de l'Eclairage), Photocarcinogenesis Action Spectrum (Non-Melanoma Skin Cancers), CIE S 019/E:2006, Vienna, 2006.
- Eck, T. F., P. K. Bhartia, and J. B. Kerr, Satellite estimation of spectral UVB irradiance using TOMS derived total ozone and UV reflectivity, *Geophys. Res. Lett.*, 22, 611-614, 1995.
- Frederick, J. E. and D. Lubin, The budget of biologically active ultraviolet radiation in the Earth-atmosphere system, *J. Geophys. Res.*, 93, 3825-3832, 1988.
- Frederick, J. E. and C. Erlick, Trends and interannual variations in erythemal sunlight, 1978-1993, *Photochem. Photobiol.*, 62, 476-484, 1995.
- Herman, J. R., P. K. Bhartia, J. Kiemke, Z. Ahmad, and D. Larko, UV-B increases (1979-1992) from decreases in total ozone, *Geophys. Res. Lett.*, 23, 2117-2120, 1996.
- Herman, J., et al., Meteor-3 Total Ozone Mapping Spectrometer (TOMS) Data Products User's Guide, NASA Ref. Pub. 1393, Goddard Space Flight Center, Greenbelt, MD, 1996.
- Herman, J. R., N. Krotkov, E. Calarier, D. Larko, and G. Labow, Distribution of UV radiation at the Earth's surface from TOMS-measured UV-backscattered radiances, *J. Geophys. Res.*, 104, 12059-12076, 1999.
- Herman, J. R., R. D. Piacentini, J. Ziemke, E. Celarier, and D. Larko, Interannual variability of ozone and UV-B exposure, *J. Geophys. Res.*, 105, 29189-29193, 2000.
- Holick, M. (Chair), R. Bouillon, J. Eisman, M. Garabedian, J. Kleinschmidt, T. Suda, I. Terenetskaya, and A. Webb, Action Spectrum for the Production of Previtamin D₃ in Human Skin, CIE Technical Report TC 6-54, Vienna, 2006.
- ICNIRP (International Commission on Non-Ionizing Radiation Protection), Global Solar UV-Index, 1995-1.
- Krotkov, N. A., P. K. Bhartia, J. R. Herman, V. Fioletov, and J. Kerr, Satellite estimation of spectral surface UV in the presence of tropospheric aerosols. 1 Cloud-free case, *J. Geophys. Res.*, 103, 8779-8793, 1998.
- Lubin, D., E. H. Jensen, and H. P. Gies, Global surface ultraviolet radiation climatology from TOMS and ERBE data, *J. Geophys. Res.*, 103, 26 061-26 091, 1998.
- MacLaughlin J.A., Anderson R.R., Holick M.F. Spectral character of sunlight modulates photosynthesis of previtamin D₃ and its photoisomers in human skin. *Science* 216(4549):1001-1003, 1982.
- Madronich, S., Implications of recent total atmospheric ozone measurements for biologically active ultraviolet radiation reaching the Earth's surface, *Geophys. Res. Lett.*, 19, 37-40, 1992.

- Madronich, S. and S. Flocke, Theoretical estimation of biologically effective UV radiation at the Earth's surface, in *Solar Ultraviolet Radiation - Modeling, Measurements and Effects* (Zerefos, C., ed.). NATO ASI Series Vol. 152, Springer-Verlag, Berlin, 1997.
- Madronich, S., R. E. McKenzie, L. O Björn, and M. M. Caldwell, Changes in biologically active ultraviolet radiation reaching the Earth's surface, *J. Photochem. Photobiol. B: Biology*, 46, 5-19, 1998.
- Mayer, B. and S. Madronich, Calculation of ultraviolet radiation quantities using TOMS ozone and ISCCP cloud data, *Eos Trans.*, 79, F170, 1998.
- McKenzie, R. L., G. Seckmeyer, A. Bais, and S. Madronich, Satellite retrievals of erythematous UV dose compared with ground-based measurements at Northern and Southern Latitudes, *J. Geophys. Res.*, 206, 24051-24062, 2001.
- McPeters, R. D. et al., *Nimbus-7 Total Ozone Mapping Spectrometer (TOMS) Data Products User's Guide*, NASA Reference Publication 1384, National Aeronautics and Space Administration, Washington, D.C. 1996.
- McPeters, R. D., et al., *Earth Probe Total Ozone Mapping Spectrometer (TOMS) Data Products User's Guide*, NASA Tech. Pub. 1998-206895, Goddard Space Flight Center, Greenbelt, MD, 1998.
- McKinlay, A.F. and B. L. Diffey, A reference action spectrum for ultraviolet induced erythema in human skin. In: Passchier W.R. and Bosnjakovic, B.F.M. (eds.) *Human Exposure to Ultraviolet Radiation: Risks and Regulations*. Elsevier, Amsterdam, 1987.
- Petropavlovskikh, I., Evaluation of photodissociation coefficient calculations for use in atmospheric chemical models, Ph. D. Thesis, U. of Brussels and NCAR/CT-159, Boulder, 1995.
- Sabziparvar, A. A., K. P. Shine, and P. M. de F. Forster, A model-derived global climatology of ultraviolet radiation at the Earth's surface, *Photochem. Photobiol.*, 69, 193-202, 1999.
- Stamnes, K., S. Tsay, W. Wiscombe, and K. Jayaweera, A numerically stable algorithm for discrete-ordinate-method radiative transfer in multiple scattering and emitting layered media, *Appl. Opt.*, 27, 2502-2509, 1988.
- UNEP (United Nations Environment Programme), *Environmental Effects of Ozone Depletion and its Interactions with Climate Change: 2002 Assessment* (van der Leun, J.C., X. Tang, and M. Tevini, eds.) United Nations Environment Programme, Nairobi, 2003.
- USSA (US Standard Atmosphere), National Oceanic and Atmospheric Administration (NOAA), National Aeronautics and Space Administration (NASA), United States Air Force, Washington DC, 1976.
- Wenny, B.N., J. S. Schafer, J. J. DeLuisi, V. K. Saxena, W. F. Barnard, I. V. Petropavlovskikh, and A. J. Vergamini, A study of regional aerosol radiative properties and effects on ultraviolet-B radiation, *J. Geophys. Res.*, 103, 17083-17097, 1998.
- WMO (World Meteorological Organization), *Report of the WMO-WHO Meeting of Experts on Standardization of UV Indices and their Dissemination to the Public*, WMO/GAW Report No. 127, Geneva, 1997.
- WOUDC (World Ozone and UV Data Center), <http://www.woudc.org/>, 2002.